POLITEHNICA UNIVERSITY OF BUCHAREST

Mechanical Engineering and Mechatronics Faculty
Mechatronics and Precision Mechanics Department

SUMMARY OF THE PH.D. THESIS

Research on the development of new sensorial modules for pneutronic systems

Author: Ing. Alina Popescu-Cuță
Leading Professor: Prof.dr.ing. Octavian Donțu

Bucharest
2020

ACKNOWLEDGEMENT

Lucrarea a fost parțial elaborată cu sprijinul proiectului strategic POSDRU/159/1.5/S/137070 (2014) al Ministerului Educației Naționale, România, co-finanțat prin Fondul Social European – Investește în Oameni, din cadrul programului Operațional Sectorial pentru Dezvoltarea Resurselor Umane 2007 – 2013.

Autoarea își exprimă recunoștința pentru susținerea oferită prin programul de cercetare PN-II-PT-PCCA-2013-4-1557, intitulat "Actuatori electromagnetici și electrodinamici obținuți prin tehnologii LIGA"

This work was partially supported by the strategic grant POSDRU/159/1.5/S/137070 (2014) of the Ministry of National Education, Romania, co-financed by the European Social Fund – Investing in People, within the Sectorial Operational Program Human Resources Development 2007-2013.

The author acknowledges the support offered through the PN-II-PT-PCCA-2013-4-1557 Research Grant, entitled "Electromagnetic and Electrodynamic Actuators Processed Through LIGA Technology"'.

TABLE OF CONTENTS

CHAPTER 1: THE THESIS OBJECTIVES

Keywords: MEMS sensor optimisation, COMSOL Multiphysics, finite element analysis.

The present-day miniaturization trends found in numerous technical and scientifical fields have grown also in the case of pneutronic systems developing new applications for these fields concerning microbiotics and biomedical engineering. These applications though require working with low pressure and flow, which demanded the development of new transducers capable of precise measuring of fluid characteristics, even when the value of these units of measure is below the normal threshold..

The first objective of this thesis is the development of some parametric numeric calculation models for the simulation of piezoresistive pressure sensors MEMS. Through the utilization of these models are obtained microsystems with optimal performance, from a measuring precision standpoint as well as the sensibility of transducers.

The second objective of this thesis consisted in the proposal of an optimization method for the performance of miniature static pressure transducers which function based on the piezoresistive principle. This proposal was sustained through the development of a numerical analysis for the constructive solution proposed and the comparison between the sensibility of these types of transducers with the ones built the classic way.

The third objective of this thesis addresses an issue often encountered in automated pneumatic systems and it is measuring the dynamic pressure of the fluid. This thesis proposes a new approach for the electromagnetic resonant sensor, which measures the dynamic pressure and speed of compressed air on the trajectory of a pneutronic system. The proposed sensor can function either in a static state, relying on the variation of the inductance of a coil, or in a dynamic state, through the measuring of variations in the resonance frequency under the influence of a fluid. Both functioning principles will be demonstrated through numerical models, and the model of functioning in a static state will be validated experimentally. Also, different future constructive solutions for the proposed sensor will be tested, both through numerical calculations and through experimental results..

CHAPTER 2. STATE OF THE ART ON THE DEVELOPMENT IN THE PNEUTRONIC SYSTEMS FIELD

2.1. General considerations

With the development in the field of microelectronics and sensory equipment, the performance of smart pneumatic systems has shown great improvements, allowing using these in new fields of activity [1]. Alongside standardized pneumatic systems, they were developed also specially designed devices, which allow the integration of sensory elements and adjustment algorithms, for obtaining the best control of these systems.

The pneutronic systems represent the answer to current automatization tendencies of pneumatics, through the integration of electronics and programing elements in classic pneumatic systems [2]. The result of this mergere consists in developing new inteligent systems, equiped with all the elements necesary for automatic control.

Although the structure of the pneutronic systems can vary based on their purpose and complexity, most intelligent pneumatic systems are composed of several basic modules,

including pneumatic actuators, sensory elements (the informational subsystem) and the command subsystem [3]. The general structure of pneutronic systems is presented in fig. 2.1.

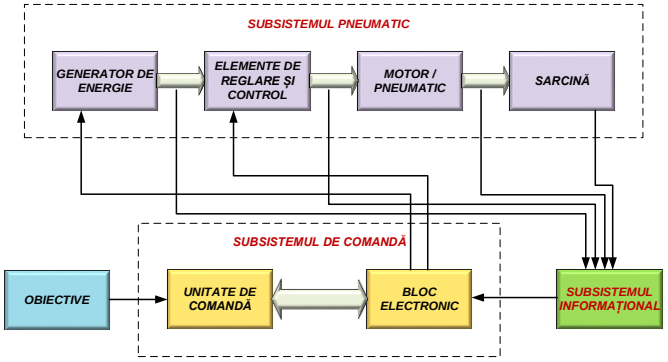

Fig. 2.1. The general structure of pneutronic systems [3]

At the base of the pneutronic systems are advanced regulation and control algorithms, for the implementation of which it is necessary to acquire in real time the specific parameters of the pneumatic process. The determination of these parameters is done with the help of sensors dedicated to each size, which then transmit the information to the system controller. Based on this information, as well as the implemented software, the controller sends commands to the system actuators, in order to carry out the regulation and control process. Currently there are two possibilities for implementing sensory elements in pneutronic systems: either as stand-alone equipment, or integrated into the structure of other equipment (cylinders, throttles, etc.). In both cases, the control and regulation accuracy of the system is closely related to the performance of the transducers, which is why current trends in the development of pneutronic systems are closely related to the optimization of sensory equipment.

To highlight the importance of sensory elements in intelligent pneumatic systems, a study was conducted of equipment and pneumatic systems that include in their structure sensors for the main process quantities (pressure, flow, temperature, position, etc.).

2.2. Pneutronic systems and equipment with integrated transducers

2.2.1 Pneutronic systems with transducers for process quantities

Pneutronic systems are used in a wide range of industrial applications, due to the many advantages they have, including: low fire risk, high working speed and compliance with hygiene and sanitation due to the absence of oil leaks or toxic substances. However, due to the compressibility of the air, the position of the load is difficult to adjust, therefore most of these systems are controlled in a closed loop, using a position reaction given by a transducer specific to this size. Also, for these systems to work properly, it is necessary to ensure a constant working pressure, which is why accurate pressure measurement is an aspect of major importance in the design and implementation of pneutronic systems.

2.2.2 Pneutronic equipment with integrated transducers

The next stage in the development of pneutronic systems was the integration of sensory elements in the system in the structure of pneumatic equipment, thus obtaining complex devices with high performance, which may even be in some cases an automatic system on its own. The purpose of introducing transducers into the structure of conventional equipment is either to reduce hysteresis (in the case of proportional distributors) or to ensure closed-loop control of the device (in the case of pressure regulators and special construction motors) [9]. Pressure regulators are essential equipment for the operation of any pneumatic system. In the case of systems that operate with compressed air, most regulators have an exhaust valve in the

atmosphere, but the classic constructions are slow and do not ensure a real-time regulation of the pressure in the system.

2.3. State of the art in the development of transducers used in pneumatic systems

The efficient operation of pneutronic systems involves real-time monitoring of several physical quantities (pressure, temperature, flow, displacement, forces, speeds, accelerations, moments) which are the main process parameters of these systems. The automatic adjustment of pneumatic automation systems is based on the precise, real-time adjustment of these parameters, which implies a more accurate knowledge of the values of the physical process quantities listed above. Consequently, current efforts to develop the field of pneutronic systems focus on two main directions: improving the characteristics of measuring devices and developing data acquisition systems.

The chapter aims to identify the main features of transducers used in pneutronic systems. The aim of this study is to develop methods to compensate for the limitations of various measurement elements to obtain the most accurate values of the physical quantities of the process.

The transducers most frequently used in automatic pneumatic systems can be classified according to [12], according to the measured quantity, as follows:

a) Transducers for mechanical units:
    - Movement transducers
    - Pozition transducers

b) Fluid transducers:

- Temperature transducers
- Flow transducers
- Pressure transducers.

2.4. Miniaturization trends in pneutronics

The introduction of sensory elements in conventional pneumatic systems has opened the possibility of operating these systems in automatic mode, which allows the use of intelligent pneumatic systems in a wide range of applications.

Current research trends in the field of drive, regulation and measurement systems focus on obtaining precise, modular, small and low cost systems. New pneutronic equipment can reach miniature dimensions and can be made with the help of micro-manufacturing technologies, even on a single silicon wafer. Their advantages are low manufacturing costs and simple construction, which increases the life of the equipment by the absence of moving components that can easily break down.

The main problem in the development of pneutronic microsystems is the work at low pressures and flows, characteristic of the equipment used. For this reason, there has been a need to develop new transducers, small enough to be successfully implemented in microsystems and offering high measurement accuracy for low pressures and flows.

The solution for obtaining these new measuring equipments appeared with the development of MEMS technologies (micro-electro-mechanical systems). MEMS type transducers are characterized by small dimensions (of the order of millimeters), constructive simplicity (which substantially reduces the cost of equipment) and the possibility of measuring very small variations of process sizes. For these reasons, MEMS sensors are the answer to the need to measure low flow rates and working pressures in micropneutronic systems.

CHAPTER 3: RESEARCH ON THE OPTIMIZATION OF PIEZORESISTIVE MEMS PRESSURE TRANSDUCERS

3.1. INTRODUCTION

The chapter studies the main aspects related to the design and simulation of the operation of piezoresistive pressure MEMS transducers, as well as aspects regarding their optimization. For this purpose, I have intensively studied the physical phenomena underlying the operation of these sensors and have performed simulations of their behavior, in order to verify the proposed optimization possibilities. In this chapter I have studied two types of elastic membranes: circular and square, these being specific to piezoresistive pressure transducers, due to the ease of their manufacturing through monocrystalline silicon etching processes.

I also determined the influence of membrane geometry on the sensitivity of the sensors by analyzing the output signal obtained for each geometry. The variations of Von Mises stresses, specific deformations and output signal for each structure and for different thicknesses of the elastic membrane have also been studied. At the same time, I determined the ideal positions of the piezoresistors on the membrane surfaces, in order to ensure the highest possible sensitivity of the transducers. In the same chapter, I developed and proposed a possibility to optimize the structure of piezoresistive pressure transducers with circular membrane, which would ensure a superior sensitivity of this equipment

3.2. THE MATHEMATICAL MODEL OF THE MEMS PIEZORESISTIVE PRESSURE TRANSDUCERS

Due to the piezoresistive properties of the sensitive elements in the structure of the pressure transducers, the deformation induced by the application of pressure on the sensor membrane produces a variation of the electrical resistance of the piezoresistors. According to [35], the variation of the electrical resistance of a piezoresistor is described by the equation:

$$R = \rho \frac{l}{A}$$

where:
l = length of the piezoresistor,
A = the cross-sectional area of the piezoresistor
ρ = resistivity of the piezoresistor material

In a more general case, if we consider the plane state of mechanical stresses but without neglecting the mechanical planar shear stress, we obtain the following relation:

$$\frac{\Delta R}{R} = \pi_l \sigma_l + \pi_t \sigma_t \tag{3.21}$$

where, according to [40], if the effect of the transverse mechanical stresses is also taken into account, the lateral and transversal piezoelectric coefficients for the <110> direction are:

$$\pi_l = \frac{\pi_{11} + \pi_{12} + \pi_{44}}{2}$$
$$\pi_t = \frac{\pi_{11} + \pi_{12} - \pi_{44}}{2} \tag{3.22}$$

The variation of the electrical resistance of the piezoresistive elements depends on the type and value of the mechanical stresses to which they are subjected and therefore on their arrangement on the elastic membrane of the sensor. There are thus two cases: piezoresistors

oriented on the x axis (fig. 3.1) and piezoresistors oriented on the y axis of the membrane (fig. 3.2).

.

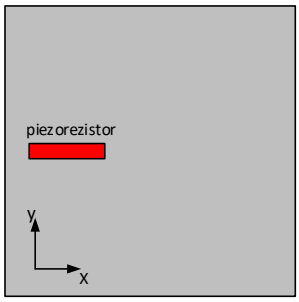

Fig. 3.1. X oriented piezoresistor

Fig. 3.1 shows an elastic membrane of a MEMS transducer, on the surface of which a uniformly distributed pressure acts. When the pressure is applied, a positive radial stress σrad, equal to σl, and a tangential voltage σtan, negative, equal to σt (σtan <0, σrad> 0) act on the piezoresistor. Therefore, according to [7], the value of the voltage σtan is described by equation 3.19, and the relative variation of the electrical resistance can be calculated using relation 3.24. In this case, the electrical resistance of the element increases with the value ΔR.

$$\sigma_{tan} = \sigma_{rad}\nu \quad (3.23)$$

$$\frac{\Delta R}{R} = (\pi_l - \nu\pi_t)\sigma_{rad} \quad (3.24)$$

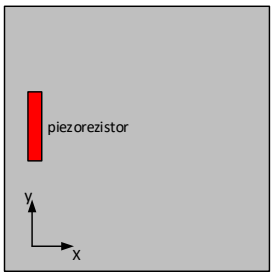

Fig. 3.2. Y oriented piezoresistor

The piezoresistor in fig. 3.2 is oriented on the y direction of the membrane, and on it acts a tangential tension σtan, positive, with the value σl and a radial tension σrad, negative, equal to σt. (σtan> 0, σrad <0).

Therefore, according to [40], the transverse voltages are described by equation 3.25, and the relative variation of the electrical resistance as a function of stress can be calculated using the relation 2.26. In this case, the strength of the element decreases.

$$\sigma_{rad} = \sigma_{tan}\nu \quad (3.25)$$

$$\frac{\Delta R}{R} = (\pi_t - \nu\pi_l)\sigma_{tan} \quad (3.26)$$

In order to be able to measure the smallest resistance variations, the MEMS piezoresistive pressure sensors have in their structure four sensitive elements of equal dimensions, arranged in a Wheatstone bridge (fig. 3.3).

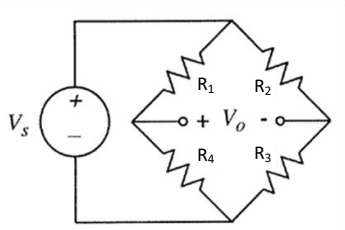

Fig. 3.3. Wheatstone bridge [40]

The Wheatstone bridge consists of two series of two resistors, connected in parallel. Using Ohm's law and Kirchoff's laws, one can write the relationship between the supply voltage of the bridge and the output voltage, as following:

$$V_0 = V_s\left(\frac{R_4}{R_1+R_4} - \frac{R_3}{R_2+R_3}\right) \tag{3.27}$$

If no pressure is applied to the membrane, the Wheatstone bridge is balanced, and V0 = 0. If V0 = 0, using the relation 3.27, the equilibrium condition of the Wheatstone bridge can be written:

$$V_0 = 0 \rightarrow \frac{R_4}{R_1+R_4} - \frac{R_3}{R_2+R_3} = 0 \rightarrow \frac{R_4}{R_1} = \frac{R_3}{R_2} \tag{3.28}$$

Under the action of pressure on the surface of the sensor membrane, each piezoresistive element registers an increase, respectively a decrease of the electrical resistance, depending on their orientation in the plane and on the mechanical stresses acting on them.

In the case of piezoresistive pressure sensors, the positioning of the sensitive elements is done in such a way as to obtain a maximum sensitivity of the transducer, so an output voltage as high as possible for a minimum value of the load. For this, it is necessary to obtain as large an imbalance as possible of the Wheatstone bridge, produced if the resistance value of two elements decreases and of the other two, increases, as will be demonstrated in the following.

Based on fig. 3.1 and 3.2, as well as relations 3.24 and 3.26, in order to obtain the increase of the resistance of a pair of elements, it is necessary to position them in the x-x direction, and in order to obtain a decrease, the positioning of the elements is done in the y-y direction. Thus, the configuration of fig. 3.4, in which the elements R2 and R4 register a decrease in electrical resistance, and R1 and R3 an increase in it.

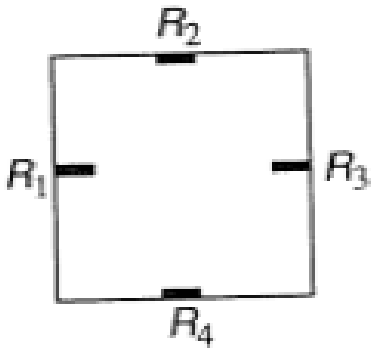

Fig. 3.4. Piezoresistors position on a pressure sensor [40]

Due to the positioning of the elements on the flexible membrane, the transverse elongation supported by resistors R2 and R4 is equal to the longitudinal elongation supported by resistors R1 and R3 and the longitudinal elongation supported by resistors R2 and R4 is equal to the transverse elongation supported by resistors R1 and R3. Due to this aspect, as well as the fact that from a dimensional point of view the piezoresistive elements are identical, the absolute value of the variation of their electrical resistance is equal for all four resistors, as follows:

$$R_1 = R_1 + \Delta R \tag{3.29}$$

$R_2 = R_2 - \Delta R$
$R_3 = R_3 + \Delta R$
$R_4 = R_4 - \Delta R$

Thus, for the configuration of the piezo resistors in the figure. 3.4, is obtained using relation 3.27, the voltage at the output of the Wheatstone bridge:

$$V_0 = V_s(\frac{\Delta R}{R}) \quad (3.30)$$

3.3. RESEARCH ON THE INFLUENCE OF ELASTIC MEMBRANE GEOMETRY ON THE PERFORMANCE OF MEMS PIEZORESISTIVE PRESSURE TRANSDUCERS.

In the following, I modeled and simulated two types of MEMS piezoresistive pressure transducers [38], which differ in the geometry of the elastic membrane: one transducer has a circular membrane and the other a square membrane. To highlight the influence of membrane geometry on transducer performance, both sensors have the same surface area and aperture thickness, as well as the same size, position, and orientation of the piezoresistors. Also, the materials that go into the structure of the sensors are similar. Therefore, since the inlet pressure is the same for both transducers, the differences in performance will come strictly from the geometry of the elastic membrane.

3.3.1. Research on the performance of a piezoresistive pressure transducer with a circular membrane

The sensor is built on a n-crystalline monocrystalline silicon wafer, measuring 5 mm x 5 mm. The total thickness of the plate is 500 μm, in which a circular membrane was positioned in the center of the plate, with a thickness of 30 μm. The membrane is embedded on the edges of the fixed frame of the sensor and, having a much smaller thickness than the rest of the plate, it will deform under the action of an inlet pressure.

The transducer model was designed entirely using the 2D and 3D module, integrated in the COMSOL Multiphysics software. Four piezoresistors, equal in size, made of p-doped silicon and connected in a Wheatstone bridge are deposited on the sensor membrane. They are 200 μm long, 50 μm wide and have a thickness of 0.5 μm. In order to differentiate them, I represented the piezoresistors in red and assigned them the notations R1, R2, R3 R4.

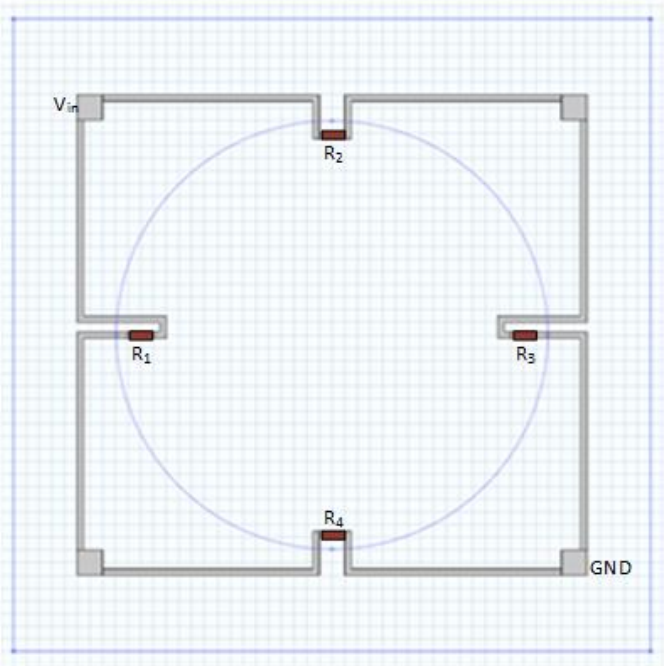

Fig. 3.6. Sensor circuit

The figure also indicates the power supply terminal of the sensor (denoted VIN) and its mass, denoted GND. To apply a 9V voltage to the circuit terminals, we used a Terminal type condition. The voltage measurement at the output of the transducer is performed between the terminals opposite the two, diagonally.

According to [40], resistors R1 and R2 will be subjected to transverse voltages, so their electrical resistance will decrease by ΔR1 and ΔR2, respectively, and R3 and R4 will increase by ΔR3 and ΔR4, respectively, due to the longitudinal voltages acting on them. Using relation (3.1), the formula for the electrical resistance of each pair of piezoresistors can be written as follows:

$$R_1 = \rho_1 \frac{l_1}{h_1 w_1}$$
$$R_2 = \rho_2 \frac{l_2}{h_2 w_2} \qquad (3.31)$$
$$R_3 = \rho_3 \frac{l_3}{h_3 w_3}$$
$$R_4 = \rho_4 \frac{l_4}{h_4 w_4}$$

where:

$\rho_{1...4}$ = material resistivity;

$l_{1...4}$ = piezoresistors length;

$w_{1...4}$ = piezoresistors width;

$h_{1...4}$ = piezoresistors thickness;

Based on the above reasoning, the strength of the pair of elements R1 and R3 will increase after deformation with ΔR, and the resistance of the pair R2 and R4 will decrease with ΔR, thus unbalancing the Wheatstone bridge and generating an output signal proportional to the deformation, so with the applied pressure .

In fig. 3.7 is presented the three-dimensional model of the pressure transducer with circular membrane, for which we determined the variation of the output signal with the inlet pressure.

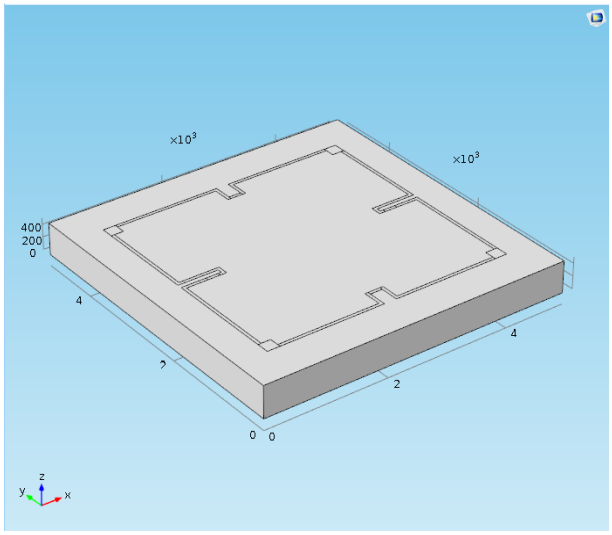

Fig. 3.7. 3D model of the sensor

To simulate the behavior of the pressure transducer, I used the Piezorezistivity and Boundary Currents module, which allows the declaration of the piezoresistive properties of the material from which the four resistors are made.

On the opposite side of the piezoresistive elements we applied a uniformly distributed pressure (fig. 3.8 a), which varies between 0.5 and 10 kPa, and we considered the sensor frame fixed (fig. 3.8 b), to simulate the behavior of a recessed membrane.

To introduce the membrane load, I used the Boundary Load option, which allows the application of force on a surface selected by the user. Although the software allows defining the mechanical load both as a point force and as a force uniformly distributed in a given direction, I opted to declare the load as pressure, so as a force evenly distributed in the normal direction on the membrane surface, due to the most accurate correspondence with reality. In order to vary the inlet pressure in a predetermined interval, we declared its value parametrically, and later we opted for a stationary study of Parametric Sweep type, imposing the initial and final values of the desired pressure range and the size variation step between the desired values.

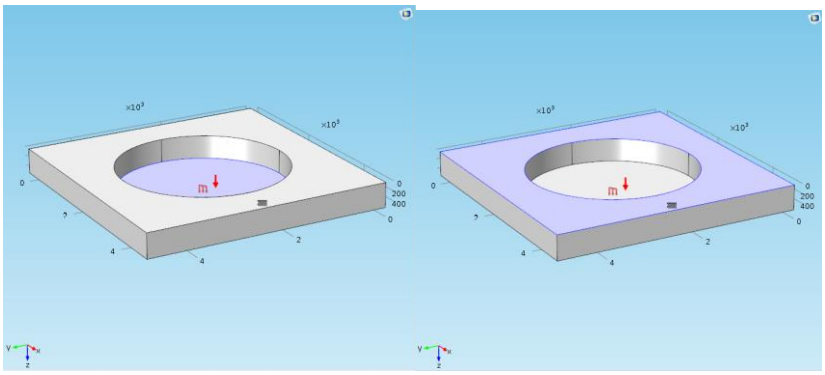

a b

Fig. 3.8.: a – pressure, b – fixed rim

Given the very small size of the structure, the shape and the minimum size of the discretization elements have a significant influence on the study results.

It is observed from fig. 3.9 that as the size of the network decreases, the output signal increases, so that the value of the output signal is maintained at small values of the network size.

The reduction of the dimensions of these elements and implicitly the increase of the network density, have as a secondary result a very long calculation time and require the use of as many hardware resources as possible. Therefore, the main objective in performing finite element calculations is to obtain a balance between the calculation accuracy and the time and resources

required to conduct the study. Therefore, given that starting with an element size of 7 μm the output signal remains unchanged, we chose this value as a discretization step for the following calculations. This option offers the best resource-accuracy ratio, the simulation result being superior in quality compared to configurations with larger elements, but close in precision to the variant with a minimum size of 1 μm, which required a long calculation time.

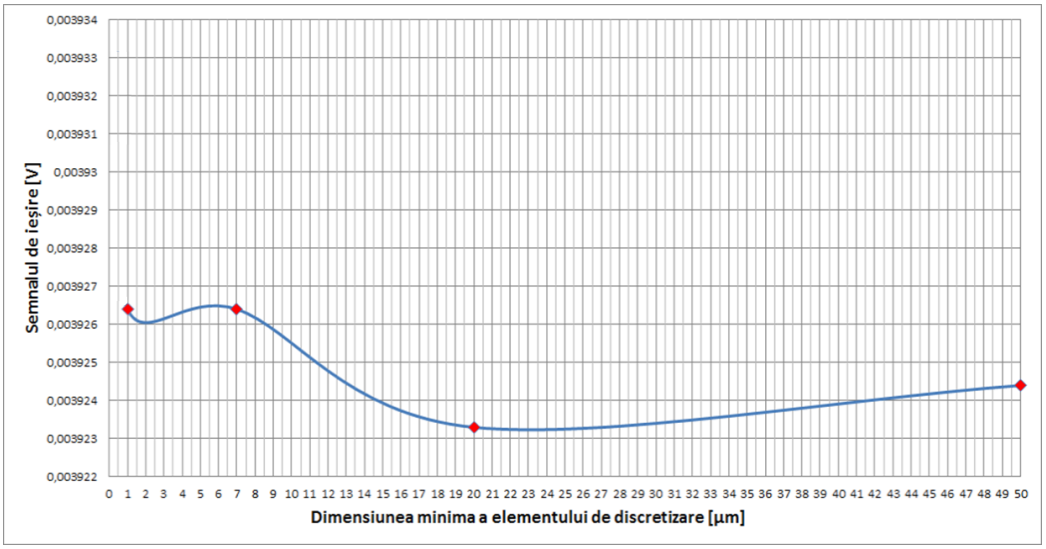

Fig. 3.9. Variation of the sensor output signal, depending on the size of the meshing elements

Therefore, a simulation of the circular membrane pressure transducer was performed, using an inlet pressure ranging from 0.5 to 10 kPa, from 0.5 to 0.5 kPa. In this configuration, the piezoresistors were positioned at 50 μm from the edge of the elastic membrane. The output signal of the transducer is shown in fig, 3.10.

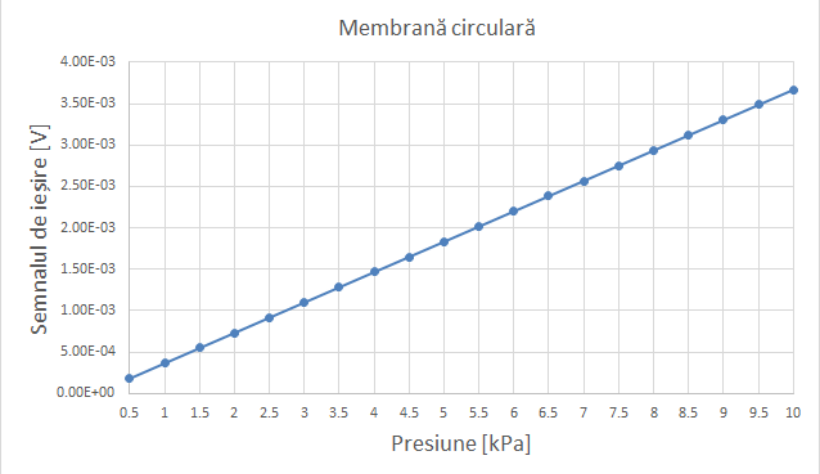

Fig. 3.10. Variation of the output signal of the circular membrane sensor, depending on the inlet pressure

3.3.2. Research on the performance of a piezoresistive square membrane pressure transducer

The configuration of the detection circuit of the square membrane pressure sensor is shown in fig. 3.11. The same notations were kept as in the case of the circular membrane sensor, as well as the same algorithm for making the three-dimensional model.

Like the sensor with circular membrane, the model was assigned as material n-doped silicon, and piezoresistors, p-doped silicon. .

The piezoresistors have the same dimensions as those used in the case of the circular membrane (200 x 50 x 0.5 μm), and the surfaces and thicknesses of the two membranes (circular and square) are equal. Also, the piezoresistors were positioned at the same distance from the edge of the membrane as in the previous case (50μm). Thus, from a geometric point of view, the different shape of the membranes represents the only difference between the two models.

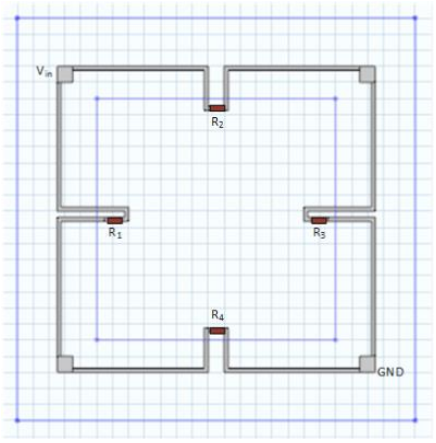

Fig. 3.11. Detection circuit on a square membrane[38]

As in the previous case, an inlet pressure with values between 0.5 - 10 kPa was evenly distributed on the lower face of the membrane, opposite the piezoresistors, and the edge around the membrane was considered fixed.

The simulation of the sensor behavior was performed for the same pressure range as in the case of the circular membrane and following the same algorithm presented previously. The dependence of the output signal on the inlet pressure sensor is shown in fig. 3.13.

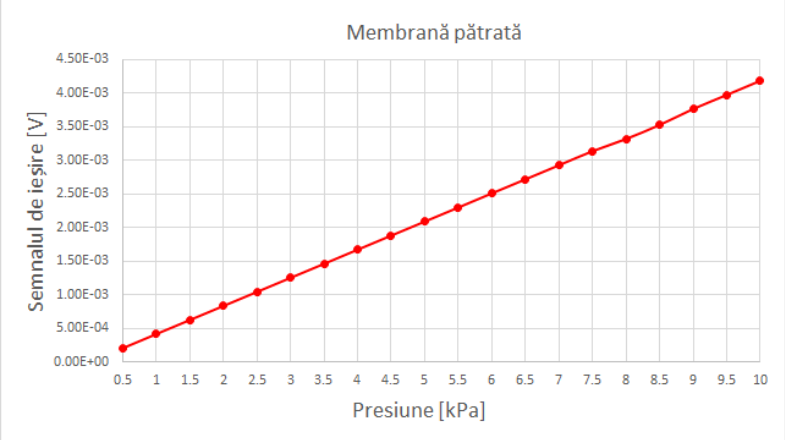

Fig. 3.13. The relation between the input pressure and the output (square membrane)

3.3.3. The influence of membrane geometry on the sensitivity of piezoresistive pressure transducers

To determine the influence of the membrane geometry of pressure piezoresistive sensors on their sensitivity, we made a comparison between the output signals of the two types of sensors, for the same values of the inlet pressure. Given that the elements are dimensionally and materially similar, the only difference between the values of the two signals is given by the geometry of the membrane. The comparison between the two obtained signals is shown in fig. 3.14.

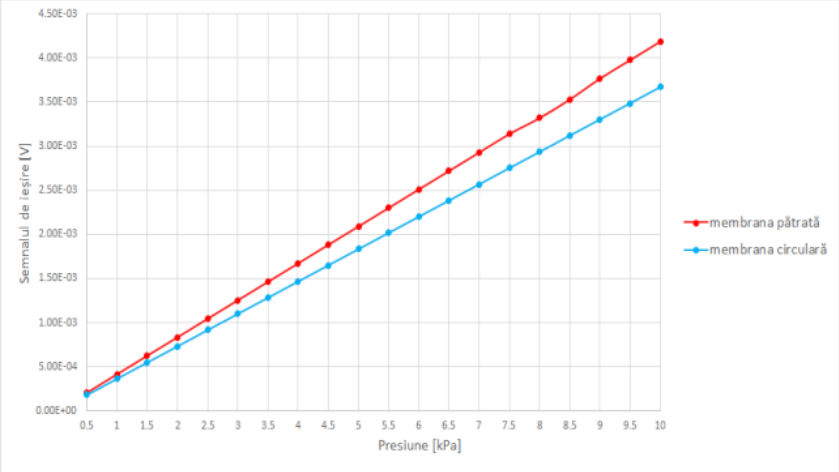

Fig. 3.14. The output signals of the two sensors [38]

In both cases of elastic membrane geometries, a linear dependence of the output signal on the inlet pressure is observed, but the output signals differ for the same value of the inlet pressure.

According to [8], the sensitivity of a piezoresistive pressure sensor is calculated using the relation:

$$S = \frac{\Delta V_0}{V_{in}} \frac{1}{\Delta P} \tag{3.32}$$

where:

V_0 = output signal of the sensor

V_{in} = input signal

ΔP = pressure variation

Given that both sensors are supplied with the same voltage (9V), and the pressure variation is the same in both models, it follows that the difference between the output signals of the transducers induces a difference between their sensitivities.

Using relation 3.32, the sensitivities for the circular membrane as well as for the square one and the relative difference between the sensitivities of the sensors were calculated.

The sensitivity of the circular membrane sensor is:

$$S_c = 4{,}0777e - 5\ [\frac{V}{bar}]$$

According to the same algorithm, the sensitivity of the square membrane sensor was calculated:

$$S_p = 4{,}6488e - 5\ [\frac{V}{bar}]$$

Relative difference in sensitivity:

$$Dif_p = 14{,}05\ \%$$

Analyzing the obtained results, it can be concluded that the square membrane ensures a higher sensitivity of the pressure sensor, compared to the circular membrane variant.

In chapter 3.2 of the paper, the dependence between the specific deformation of a piezoresistive material and the variation of its electrical resistance was highlighted, as well as the relationship between stresses and deformations, described by Hooke's law. In conclusion, the response of a piezoresistive pressure transducer and therefore its sensitivity depend on the mechanical stresses and specific deformations produced in the surface of the membrane on which the piezoresistive elements are mounted.

In view of the results obtained previously and shown in fig. 3.14, which denotes a relevant difference in sensitivity between the circular membrane sensor and the square membrane sensor, it was necessary to determine the causes that lead to this difference, in order to identify the

optimization possibilities of the sensors. For this purpose, the distribution of mechanical stresses and specific deformations in both membranes were determined.

Fig. 3.15 shows the specific deformations of the circular membrane, on the Ox and Oy axes, as well as the distribution of Von Mises stresses on the membrane surface.

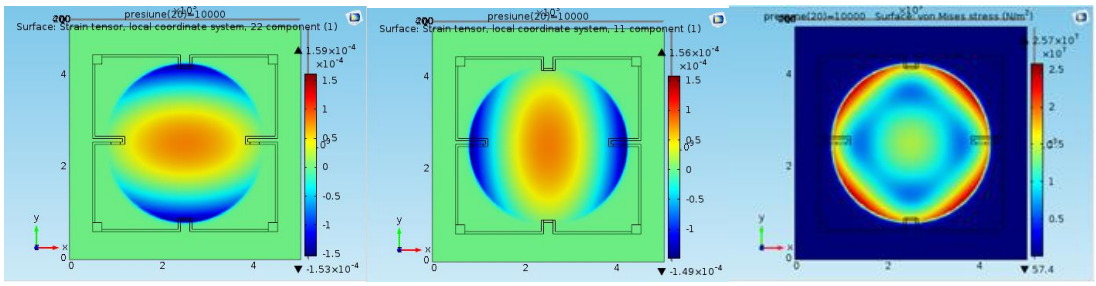

Fig. 3.15. Specific deformations and distribution of Von Mises stresses in the round membrane

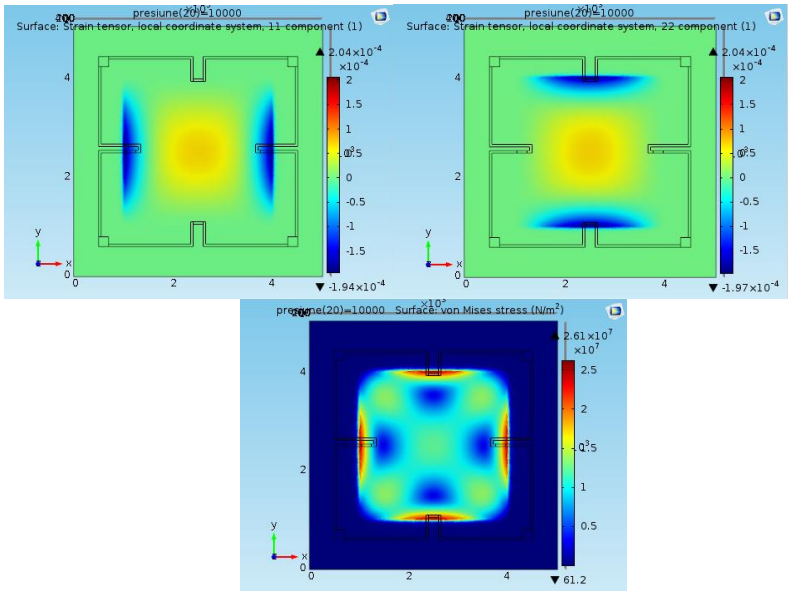

Fig. 3.16. Specific deformations and distribution of Von Mises stresses in the square membrane

From fig. 3.15 can be seen a change in the distribution profile of mechanical stresses near the piezoresistors of the circular membrane, which indicates that they, although only 0.5 μm thick, exert a stiffening effect on the membrane, which could adversely affect the performance of sensors.

In support of this statement, I performed simulations of both types of membranes, at the same inlet pressure, this time without piezoresistive elements. The distribution of Von Mises stresses in membranes is shown in fig. 3.17.

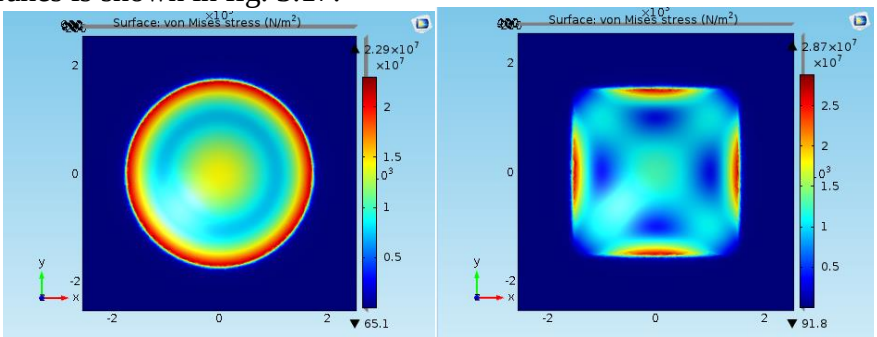

Fig. 3.17. Distribuția tensiunilor Von Mises în membrana circulară și pătrată [38]

I therefore conclude that, for a simple circular membrane, the Von Mises stresses reach maximum values around the embedded edge. By comparison with fig. 3.15, it can be seen that

the piezoresistive elements influence the distribution profile of the Von Mises stresses in the circular membranes. The stiffening effect produced by the piezoresistors becomes problematic, because the values of the mechanical stresses are maximum outside the surface of the sensitive elements, and next to the piezoresistors the Von Mises stresses reach minimum values.

To determine whether this is the cause of the difference in sensitivity between the two sensors, it is necessary to analyze the relationship between the variation of the electrical resistance and the Von Mises stress.

According to [41], the equation for Von Mises stress is:

$$\sigma_{vonMises} = \sqrt{\frac{(\sigma_{xx} - \sigma_{yy})^2 + {\sigma_{xx}}^2 + {\sigma_{yy}}^2}{2}} \tag{3.33}$$

Rezultă:

$$\sigma_{vonMises} = \sqrt{{\sigma_{xx}}^2 + {\sigma_{yy}}^2 - \sigma_{xx}\sigma_{yy}} \approx |\sigma_{xx} - \sigma_{xx}| \tag{3.34}$$

Relation 3.13 describes the dependence between stresses and specific deformations. Therefore, using relations 3.13 and 3.34, we can write:

$$\sigma_{vonMises} \approx \left|\frac{E}{1+\nu}(\varepsilon_{xx} - \varepsilon_{yy})\right| \tag{3.35}$$

Given that the variation of the electrical resistance of the sensitive elements is a result of the membrane deformation, and the values of Von Mises stresses depend, according to relation 3.35, on the difference between the deformations on the two axes of the membrane plane, it can be concluded that the sensitivity of the pressure sensor depends on Von Mises voltage values at piezo resistors.

Due to the fact that piezoresistors change the distribution of Von Mises stress in membranes, and the points where the voltages are maximum are outside the sensitive elements in the case of the circular membrane, there is a decrease in sensitivity of this type of sensor compared to the square membrane model.

3.4. DEVELOPMENT OF COMPUTATIONAL PARAMETRIC MODELS FOR DETERMINING THE OPTIMAL PARAMETERS OF THE PIEZOSISTIVE PRESSURE SENSOR MEMBRANES

As previously demonstrated, the sensitivity of MEMS-type piezoresistive pressure transducers is influenced by the specific deformations of the sensor membranes and by the distribution of mechanical stresses that lead to these deformations. According to the mathematical model presented in subchapter 3.2, the higher the values of the mechanical stresses in the elastic membranes, the higher the output signal of the transducers. Therefore, in order to develop a sensor sensitive to low pressures, it is necessary to determine the appropriate value of the thickness of the elastic membrane, so that it deforms considerably at the lowest values of the inlet pressure, but without yielding under the action of mechanical stresses. . In addition, in order to ensure the highest possible sensitivity of the sensors, it is necessary to position the piezoresistors at the points where the mechanical stresses produced by the inlet pressure reach the highest values, so that the ratio between the value of the output signal and the value of the inlet pressure is maximum. .

The calculation models that we have developed and presented in this subchapter have been defined parametrically, so that they can be adapted according to the constructive requirements of each application. By using such a model to simulate the behavior of the sensors, maximum

performance of these devices can be obtained, eliminating potential errors from the design phase and thus increasing the productivity of the manufacturing process..

3.4.1. Optimization of membrane thickness

According to [42], the maximum allowable stress of silica processed by anisotropic corrosion is 300 MPa. Therefore, the maximum values of the Von Mises stress developed in the sensor membranes must be below this resistance limit.

To determine the optimal thickness of the membranes, we used the models with circular and square diaphragm, respectively, previously developed. The pressure range set for the proposed sensors is 1… 10 kPa. Therefore, the maximum load that the membranes must withstand is 10 kPa. In order to determine the optimal membrane thickness of each sensor, we conducted a study of the variation of Von Mises stress for membrane thicknesses from 6 to 30 µm, at the maximum value of the inlet pressure.

It was observed that membranes with a thickness of 6 and 9 µm, respectively, yield under the action of a pressure of 10 kPa. The minimum thickness of the stress-resistant membranes is at the intersection between the Von Mises voltage graph and the maximum allowable voltage graph. The x-axis coordinate of the intersection point is determined using Excel software to be 12 µm. Therefore, for the given pressure range (0-10 kPa), the minimum thickness of the circular membrane of the sensor is 12 µm.

3.4.2. Optimization of pressure sensors with circular and square membrane, in terms of position of the piezoresistors

We have previously demonstrated the dependence of the output signal of pressure sensors on the variation of Von Mises stress. Therefore, according to the distribution of the voltages in the circular and the square membrane, the high sensitivity of the pressure sensors is ensured by the positioning of the piezoresistors as close as possible to the embedded edge of the elastic membrane.

In order to determine as accurately as possible the optimal position of the piezoresistors, we performed simulations of the behavior of the sensors, varying the position of the piezoresistors, from the edge to the center of the elastic membranes. All simulations were performed at an inlet pressure of 10 kPa, for the optimal membrane thicknesses, previously determined.

The position of the piezoresistors on the two membranes was varied over a distance of 50 to 1200 µm from the embedded edge, and the thickness of the membranes was set at 12 µm.

The distribution of Von Mises stress in the two membranes, under the action of an inlet pressure of 10 kPa, is shown in fig. 3.19. It can be seen from the figure that, in the case of a membrane with a thickness of 12 µm, the stresses reach maximum values near the embedded edge.

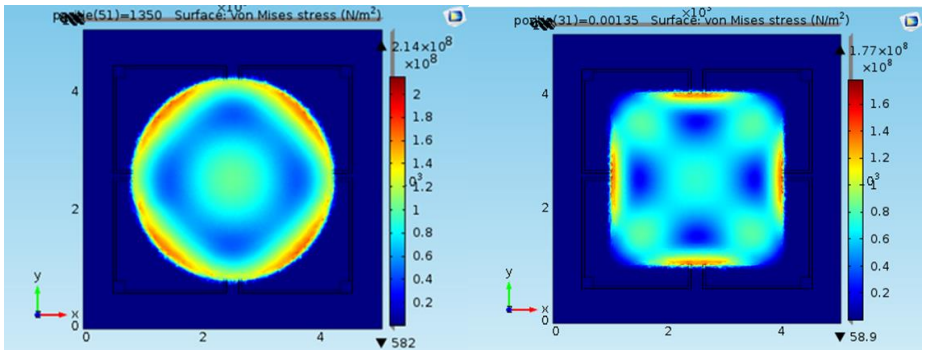

Fig. 3.18. Von Mises variation in the two membranes

I then evaluated the maximum values of Von Mises stress at the piezoresistors, for their various positions, as well as the output signal of the two sensors for each position of the sensitive elements. The obtained results are presented in fig. 3.19 and 3.20.

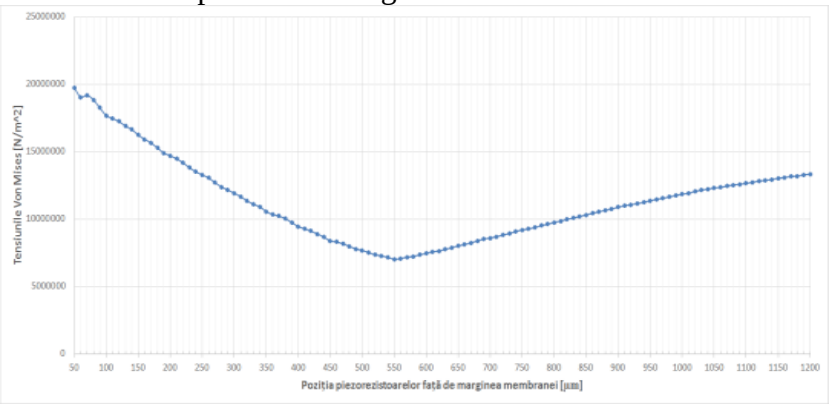

a

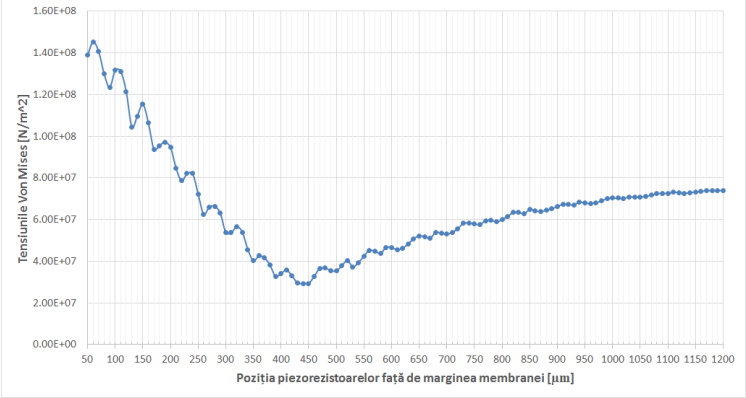

b

Fig. 3.19. . Variation of Von Mises at piezo resistors, depending on their position (a - circular membrane, b - square membrane) [38]

In fig. 3.19 a decrease of the Von Mises stress at the piezoresistors can be observed, once they move away from the recessed edge of the membrane, after which a slight increase of them near the center of the membrane.

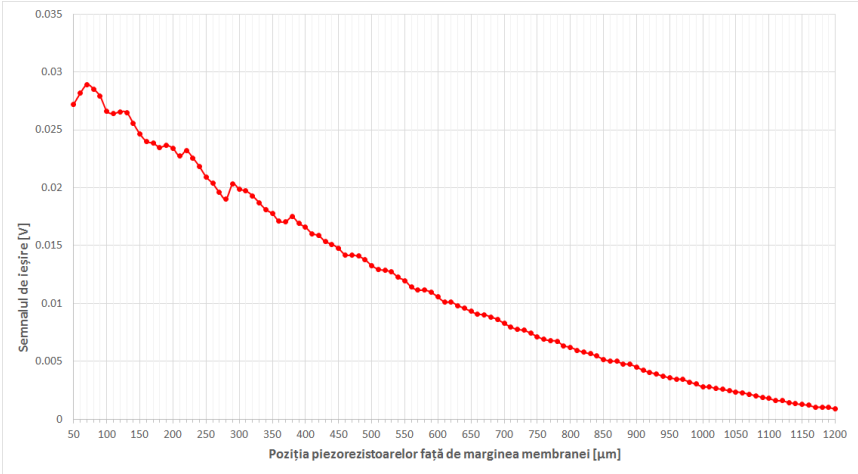

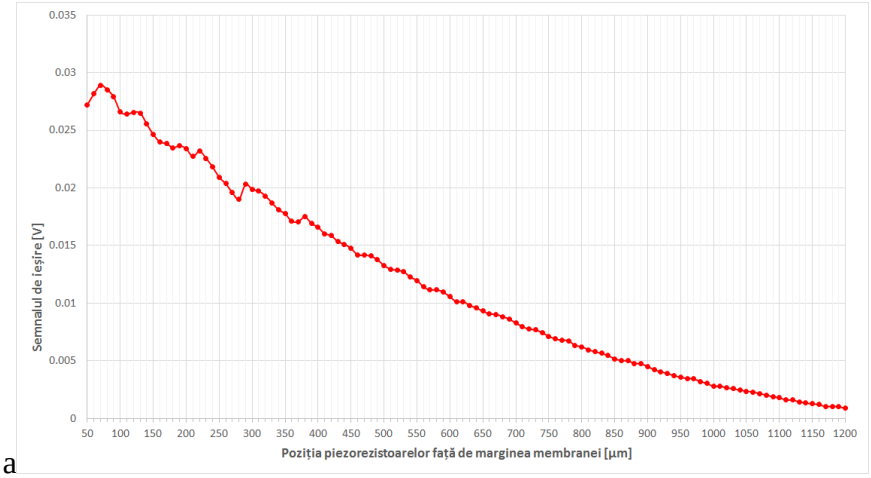

a

Fig. 3.20. Variation of the output signal of the sensors, depending on the position of the piezoresistors on the elastic membrane (a - circular membrane, b - square membrane) [38]

Because the increase in Von Mises stress to the center of the membrane is not significant enough to match the initial values, the highest values of the output signals are obtained for piezoresistors positioned near the edge of the membrane. According to fig. 3.20, the optimal position of the piezoresistors for a maximum sensitivity of the sensors is at 70 µm from the recessed edge of the membrane.

3.5. STRUCTURAL OPTIMIZATION OF CIRCULAR MEMBRANES, IN ORDER TO INCREASE THE SENSITIVITY OF PRESSURE SENSORS

Following the studies in subchapter 3.3, we concluded that the sensitivity of circular membrane pressure transducers is lower compared to sensors with a square elastic membrane, due to the variation of Von Mises stress distribution in the membrane surface, produced by the stiffening effect of piezoresistors. Therefore, we have developed a new structural approach to the circular membrane, which ensures an increase in the sensitivity of these sensors compared to their classic version.

To date, piezoresistive pressure sensors have been designed with a uniform thickness of the elastic membrane, regardless of its geometry. The proposed constructive solution involves the realization of a step of thickness with circular shape, in the surface of the membrane. The diameter of the step was defined as a percentage of the membrane diameter.

Several configurations of the sensor, with various depths and diameters of the thickness step have been simulated, to determine which configuration provides the best ratio between the maximum mechanical stresses and the output signal, as well as superior performance to the membrane of uniform thickness. I therefore calculated using finite element analysis Von Mises stress and output signals for step diameters between 10 and 95% of the membrane surface and depths of h = 3, 6, 9, 12, 15, 18, 20, 21 µm. All simulations were performed for an inlet pressure of 10 kPa, and the stress values were compared with the previously mentioned resistance limit [43].

In fig. 3.22 we presented the variation of the Von Mises stress and the output signal for each diameter of the thickness step and each its depth.

I noticed a significant increase in the values of Von Mises stresses with the depth of the step, for diameters over 40% of the original diameter of the membrane. However, the value of the output signal does not increase until the step reaches the piezoresistors and the mechanical stresses are concentrated in the active area of the sensor.

Because the 18 µm depth step induces the appearance of mechanical stresses well below the resistance level of the sensor, and the 21 µm depth step exceeds the safety limit, the optimal step depth is 20 µm.

In order to validate the proposed optimization solution, a comparison was made between the Von Mises stress and the output signals provided by a membrane with optimal uniform thickness, at an inlet pressure of 10 kPa and those obtained with the new constructive variant of the membrane, at a step depth of 20 µm, for the same value of the inlet pressure. Since the value of the output signal increases with the diameter of the membrane, according to fig. 3.22, the comparison was performed for a step diameter of 95% of the membrane diameter value.

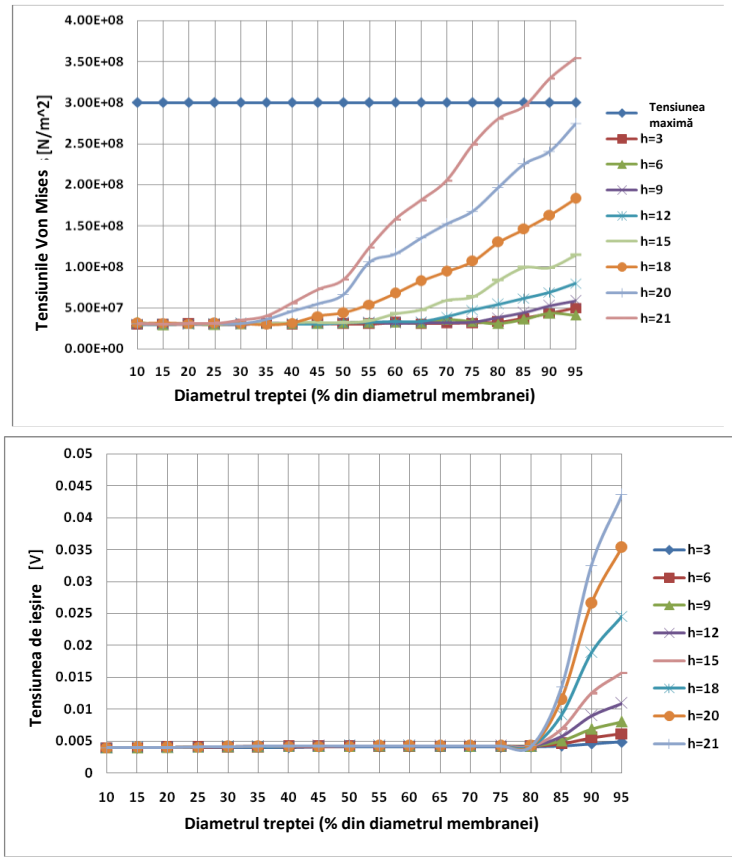

Fig. 3.22. Von Mises stress variation and output signal for each diameter and depth of the thickness step [43]

The maximum values of the Von Mises stress and the output signal for both configurations are shown in Table 1 [43].

Tabelul 1 – - Comparison between Von Mises stress and the output signal obtained in the classic membrane version, respectively in the optimized version.

	Von Mises [N/m^2]	Output [V]
Membrane with optimal uniform thickness (12 µm)	2.74E+08	0.026350
Membrane with step thickness (depth 20 µm, diamet 95% of the original)	2.74E+08	0.035338

Table 1 shows a significant difference between the output signals provided by the two types of membranes at the same inlet pressure. According to the obtained results, the proposed constructive solution confers a higher sensitivity of these sensors, compared to the classic variants.

CHAPTER 4: RESEARCH ON MODELING AND SIMULATION OF A RESONANT ELECTROMAGNETIC PRESSURE SENSOR

4.1. SENSOR OPERATING PRINCIPLE

The paper presents a new variant of resonant pressure sensor, which can be used in two ways: with electromagnetic actuation or with electromagnetic detection of pressure variation. The proposed sensor consists of two slats in the console, provided at the free ends with a matrix of permanent magnets, respectively a flat spiral coil. The lamella at the end of which the coil is located is fixed, and the one provided with magnets is flexible. The residual induction of the magnets is oriented along the Ox axis, in the xOy plane. The three-dimensional model of the sensor developed was made using Solidworks 2015 and is shown in fig. 4.1.

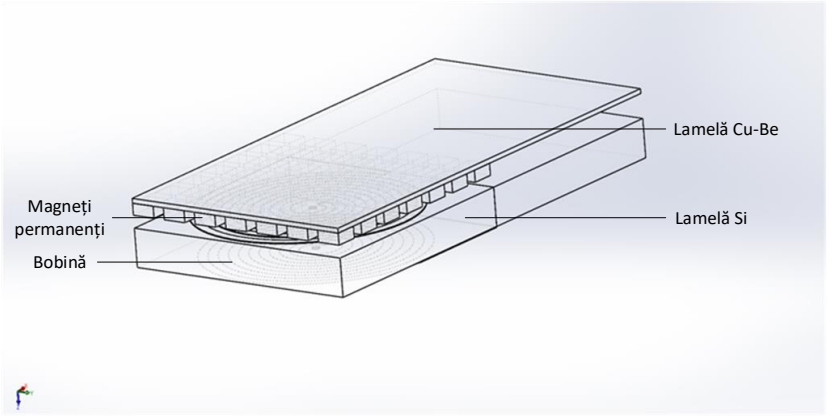

Fig. 4.1. Resonant pressure sensor with electromagnetic actuation

The flexible sensor lamella is made of a copper-beryllium alloy, the coil support plate is made of silicon, the neodymium magnets doped with boron ions, and the copper coil. The properties of the materials used are shown in Table 1.

Material	Modulul Young [GPa]	Constanta Poisson ν	Densitatea masă [kg/m^3]	Permeabilitatea megnetică relati μ_r	Inducția remanentă [T]	Permitivitatea electrică ε_r	σ [S/m]
Cu-Be	102	0,3	8250	1	-	3,4	1163
Si	168	0,22	2329	1	-	12,1	-
Cu	117	0,35	8700	1	-	1	5,998e7
NdFeB	414	0,28	7000	1,1	1,3	1,05	0.66e6

In the operation mode with electromagnetic actuation, an adjustable current is introduced in the spiral coil, thus obtaining an electromagnetic field that interacts with that of the permanent magnets. Following the interaction between the two fields, a deflection of the flexible lamella occurs. For maximum system efficiency, the flexible lamella is brought to resonant frequency by introducing a sinusoidal signal into the coil. Following the introduction of the assembly into an air flow, the pressure exerted on the flexible lamella will induce a variation of its resonant frequency. The variation of the resonant frequency of the lamella thus indicates the value of the absolute pressure of the enclosed air.

The second mode of operation of the sensor is static and is based on the variation of the inductance of a coil with its electromagnetic field [10]. Both sensor blades are at rest and the system is introduced into an airflow. The dynamic air pressure causes a deformation of the blade with the matrix of permanent magnets, which results in a variation of the magnetic flux in the

coil, due to the change in the distance between the two blades of the sensor. The result is a variation of the coil inductance, which can be detected by means of an oscillating circuit.

4.2. MODELING THE PROPOSED SYSTEM

Numerical modeling of the system was performed using the finite element method and COMSOL Multiphysics software. The realization of the proposed resonant sensor model involves solving several problems that take place on 3D computing domains. A simplified model of the system was proposed, in which the action of physical phenomena was considered unidirectional: the distribution of electric current in the coil is not influenced by the magnetic field, and the magnetic field does not vary with the structural deformations. Therefore, it is necessary to initially model the system in steady state and solve the problems of electric and magnetic field, in order to determine the electromagnetic interaction force between the coil and the matrix of permanent magnets.

4.2.2. Modeling and simulation of the sensor in the version with electromagnetic drive, using COMSOL Multiphysics

After realizing the three-dimensional model and defining the initial conditions, I proceeded to solve the problem of electromagnetism, structured in several stages. The first stage of modeling consists in determining the current density distribution in the coil, after which the magnetic field problem is solved, respectively the determination of the electromagnetic force. The deformation induced by the action of force on the permanent magnet lamella is initially determined in steady state, after which a modal analysis of the system is performed, calculating the values of resonant frequencies for the first six vibration modes of the flexible lamella. Subsequently, the variation of the resonant frequencies under the action of a fluid is highlighted and the law of variation of the frequency with the inlet pressure is calculated. We also made a modal model of the system.

4.2.2.1. Importing the CAD model and defining the initial parameters

Thanks to the Livelink for Solidworks option, implemented in the COMSOL 5.0 software, the import of the previously made CAD model was possible using the Geometry - Import -3D CAD File command (fig. 4.2). The workspace has been set to 3D and the lengths to mm.

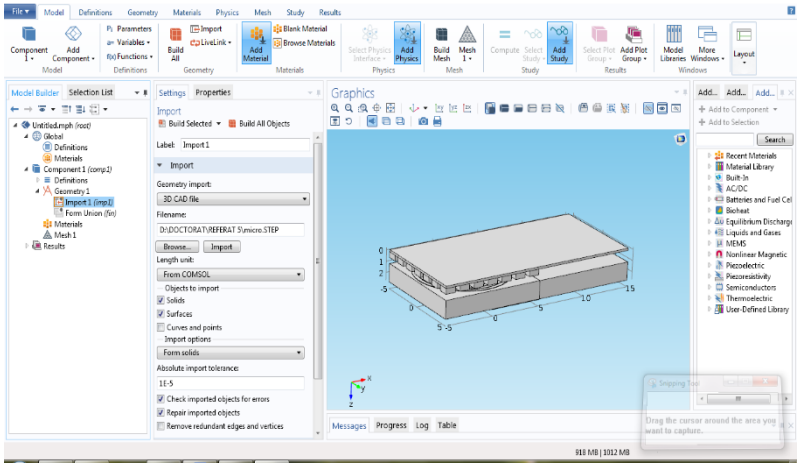

Fig. 4.2. Importing the CAD model from Solidworks

In addition to the geometry of the sensor, a circumscribed sphere has been added to it, to which air has been assigned as material and which is necessary for the delimitation of magnetic field lines.

After importing the model, the initial parametric quantities were declared. In a first stage, using the command Definitions - Parameters - Add parameter, the value of the electric voltage at the coil terminals (Ub = 0.022 V), necessary for solving the electrokinetic field problem (fig. 4.4), was defined. All other initial parameters used later in the simulation of the system during this work were defined by the same method.

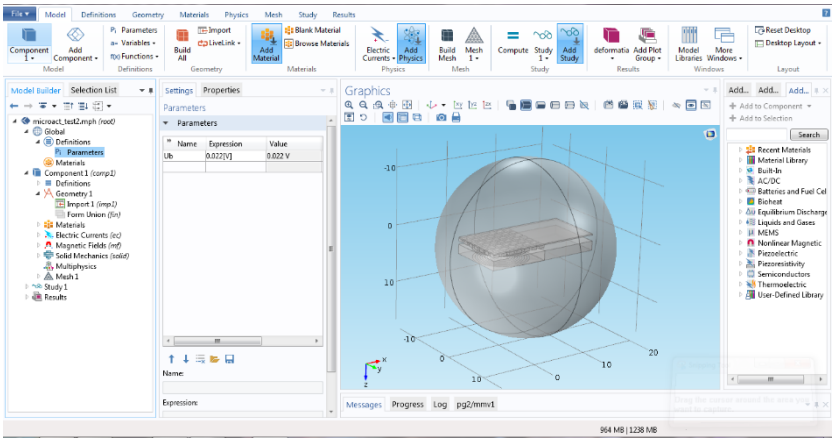

Fig. 4.4. Declaring the initial parameters

4.2.2.2. Assignment of materials

The addition of materials in the modeling of the electromagnetic system is done with the command Materials - Add material. Each material is then assigned to the corresponding domain (fig. 4.5), and their properties correspond to table 1.

COMSOL offers the possibility to use materials with predefined properties, available in its own material library, as well as materials whose properties are fully defined by the user. When using a predefined material, any of its properties is editable, without affecting the rest of the characteristic constants. If you want, instead, to use a non-existent material in the COMSOL database, whose characteristics are known to the user, it is recommended to use the command Materials - Add blank material.

4.2.2.3. Solving the electric field problem

The electrokinetic field problem aims to determine the current density in the coil. For this, the Electric Currents module is used, defined on all areas of the 3D model. The declaration of the electric voltage on the coil was made by adding an Electric Potential condition to one of the coil terminals and a Ground condition (V = 0) to the other. The value of the electric potential at the coil terminals is declared by the condition Electric Potential, using the parameter Ub, defined in the first stage of the simulation.

To solve all three problems (electrokinetic, magnetic and structural), a Stationary study was used, considering all the declared and calculated quantities as constant over time. Following the solution of the electrokinetic field problem, the current density in the coil resulted, shown in fig. 4.8.

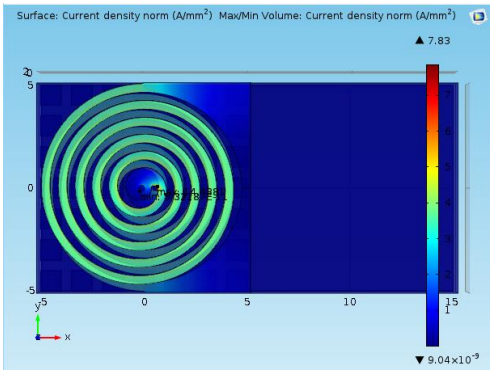

Fig. 4.8. Current density in the coil

4.2.2.4. Solving the magnetic field problem

Solving the magnetic field problem aims to determine the magnetic induction and electromagnetic interaction force between the coil and the permanent magnet matrix. The determination of the electromagnetic force is necessary to solve the structural problem, which is responsible for the deformation of the moving slide.

The definition of the magnetic problem is done using the Magnetic fields (mf) module, introduced using the Add physics - Magnetic fields (mf) command.

The magnetism problem is defined on all areas of the model, the delimitation of the field lines being made with the help of the air sphere.

The definition of magnets is done with an Ampere's Law type condition, applied on the domain of the element matrix. Under the same condition is specified the orientation of the remaining induction of the magnets, Br, in the xOy plane, in the direction Ox

The closure of the field is obtained by declaring a condition of magnetic insulation on the contour of the sphere. The condition is accessed from the Physics - Boundaries - Magnetic Insulation menu.

To solve the magnetism problem, it is necessary to introduce the current density into the coil, using an External Current Density condition, applied to the coil domain. The values of the current density in the directions Ox, Oy and Oz, resulting from the electric field problem are specified in the condition.

The components of the current density on the three axes are taken from the section Results - Expression - Electric currents - Currents and charge - Current density (Spatial), and the names of the variables (ec.Jex, ec.Jey, ec.Jez) are entered in the condition from fig. 4.12.

The calculation of the electromagnetic force that will produce the deformation of the movable slide is performed by applying a Force Calculation type condition on the coil domain. Since the lamella provided with the coil is fixed, the electromagnetic force of interest is that exerted by the conductor on the lamella provided with magnets. The direction in which the force acts is specified in the Torque Axis field, with the help of which the direction of Oz was determined by the force.

Due to the very small diameter of the electrical conductor, the coil was discretized using a smaller finite size compared to the rest of the system. Given the spiral structure of the coil, as well as its reduced thickness, a Swept type discretization was used, using triangular elements with a maximum size of 0.3 mm.

The results of the magnetic field problem consist in the display of the magnetic field lines (fig. 4.16) and the determination of the electromagnetic interaction force between the coil and the magnets, presented in fig. 4.17.

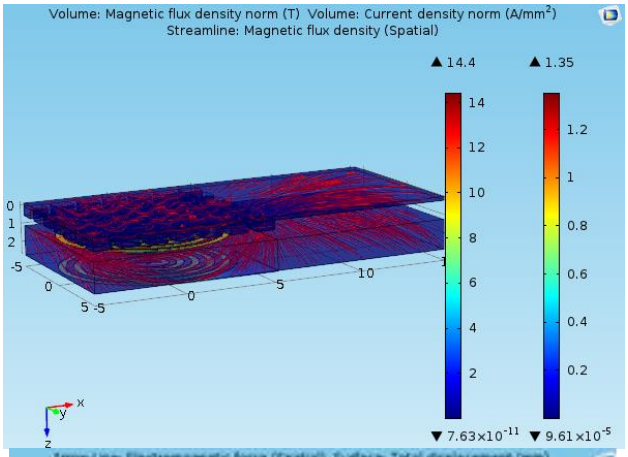

Fig. 4.16. Magnetic field lines

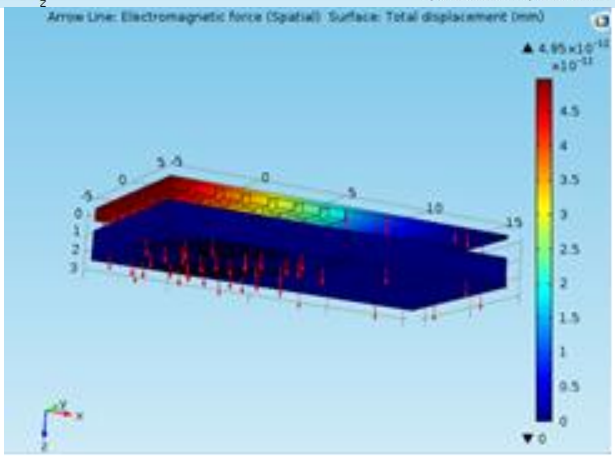

Fig. 4.17. Electromagnetic force

4.2.2.5. Solving the structural problem

The proposed sensor operates in dynamic mode, therefore it is necessary to determine the deformations of the movable slide for several resonant frequencies, respectively several vibration modes.

The first six vibration modes and resonant frequencies of the moving slide were initially determined in the absence of any loading. For this purpose, it was necessary to use the Solid Mechanics module, together with an Eigenfrequency study.

The slide with the coil was considered fixed, together with the base of the movable slide, using a Fixed Constraint condition

The next stage of the structural problem was to determine the influence of air pressure on the resonant frequencies of the moving slide.

To make the model, it was necessary to introduce electromagnetic force as a force of volume acting on permanent magnets and air pressure exerted on the movable slide. After solving the structural problem, the law of variation of the resonant frequency of the lamella will be determined according to the value of the inlet pressure.

The values of the electromagnetic force in the directions Ox, Oy and Oz were obtained after solving the magnetic field problem. It was necessary to define three interpolation functions (called forzax, fortay and fortaz), for the components of the electromagnetic force on the three spatial axes.

The electromagnetic force is then defined as a charge on the magnet field, using a Body load condition. The components of the force on the three axes are declared using the name of the corresponding interpolation functions.

The pressure exerted by the air flow is then declared using a Boundary load condition, on all the free surfaces of the movable lamella, the lamella provided with the coil being considered fixed. The air pressure value was declared parametrically.

The next stage of the simulation was to perform a parametric study of Prestressed Analysis - Eigenfrequency, to determine the variations of the resonant frequency of the sensor blade, under the simultaneous action of electromagnetic force and external pressure. The first six eigenfrequencies of the moving slide were determined for inlet pressure values between 1 and 10 kPa, with a pitch of 0.5 kPa.

In fig. 4.23 graphically represents the variation of the first six resonant frequencies of the moving slide, depending on the inlet pressure.

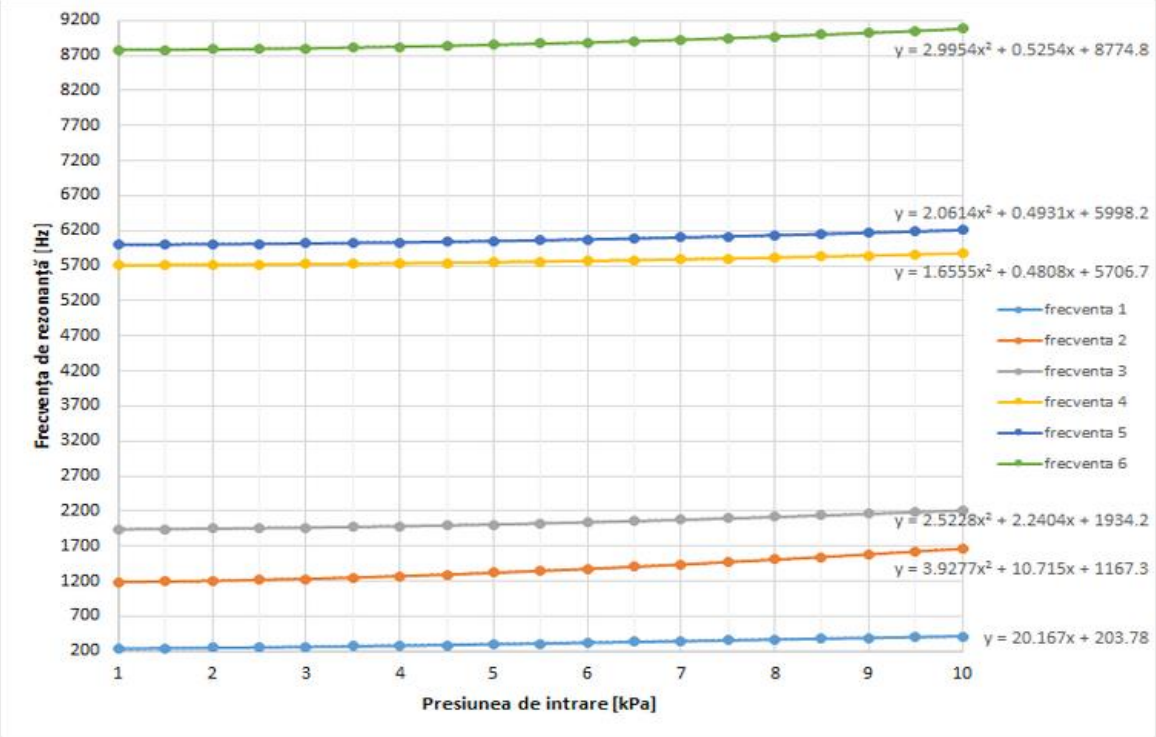

Fig.4.23. Variation of resonant frequencies depending on the inlet pressure

The law of variation of each frequency with the inlet pressure is presented next to each curve on the graph in fig. 4.23. The only case in which the variation of the resonant frequency with the inlet pressure takes place according to a linear law is for the first vibration mode, at a frequency of 236, 51 Hz.

4.3 THE MATHEMATICAL MODEL OF THE DYNAMIC SYSTEM

Având în vedere funcționarea în regim dinamic a senzorului, a fost necesară determinarea parametrilor modali pentru modul de vibrație de interes al elementului mobil. Acești parametri (masa, constanta elastică și amortizarea) sunt apoi utilizați pentru a dezvolta modelul modal al senzorului.

Senzorul studiat se încadrează în categoria sistemelor cu un singur grad de mobilitate (fig. 4.24), unde x este deplasarea lamelei mobile a senzorului, iar x_b, deplasarea bazei).

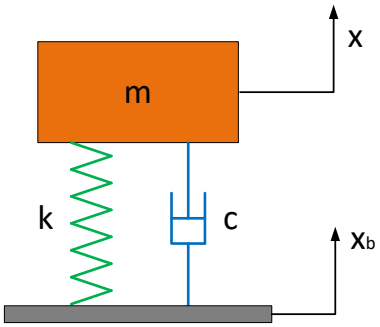

Fig. 4.24. The model of a system with a single degree of freedom

The equilibrium equation of a system with a single degree of freedom is [58]:

$$m\ddot{x}(t) + c\dot{x}(t) + kx(t) = f(t) \quad (4.1$$

Where:
m = the modal mass of the system,
c = depreciation,
k = elastic constant,
f(t) = external forces acting on the system,
After applying d'Alembert's principle, according to which the sum of forces is zero at any given time, the homogeneous form of the equation is obtained. (4.15):

$$m\ddot{x}(t) = -c\dot{x}(t) - kx(t) \quad (4.1$$

The frequency system model is a link between the calculation model and the experimental results and is based on the transfer function which represents the force-displacement ratio of the system [58]:

$$X(\omega) = H(\omega) \cdot F(\omega) \quad (4.1$$

Prin aplicarea unei transformate Fourier relației (4.15), se obține forma algebrică a ecuației diferențiale inițiale, astfel:

$$(-m\omega^2 + j\omega c + k) \cdot X(\omega) = F(\omega) \quad (4.1$$

Where:

$$-m\omega^2 + j\omega c + k = B(\omega) \quad (4.1$$

B (ω) = system impedance.
From the relations (4.17), (4.18) și (4.19), results:

$$B(\omega) = \frac{1}{H(\omega)} \quad (4.2$$

And:

$$H(\omega) = \frac{1}{-m\omega^2 + j\omega c + k} \quad (4.2$$

During the testing process, the sensor was placed on a piezoelectric actuator, controlled by a sinusoidal voltage signal. In the absence of a second measurement reference at the base of the slide, the following can be written for the measured system:

$$m\ddot{x} = -k(x - x_b) - c(\dot{x} - \dot{x_b}) \quad (4.2$$

$$\frac{\dot{x}}{U} = \frac{\dot{x}}{\dot{x_b}} \cdot \frac{\dot{x_b}}{U}$$

Where:
x = moving of the tip of the sensor lamella,
x_b = moving of the base of the lamella.
U = input voltage
From (4.22) results:

$$x(-m\omega^2 + j\omega c + k) = x_b(k + j\omega c) \quad (4.2$$

The relation (4.23) can be written as:

$$\frac{x}{x_b} = \frac{k + j\omega c}{-m\omega^2 + j\omega c + k} \quad (4.2$$

The system transfer function can be written as:

$$H(\omega) = \left|\frac{\dot{x}}{\dot{x_b}}\right| = \frac{\sqrt{k^2 + \omega^2 c^2}}{\sqrt{(k - m\omega^2)^2 + \omega^2 c^2}} \quad (4.2$$

From the equations (4.22) și (4.26), results:

$$H(\omega) = \frac{\dot{x}}{U} / \frac{\dot{x_b}}{U} \quad (4.2$$

The speed of the lamella and its embedded base were determined experimentally, using laser vibrometry and the experimental stand described in detail in chap. 5. (fig. 4.25)

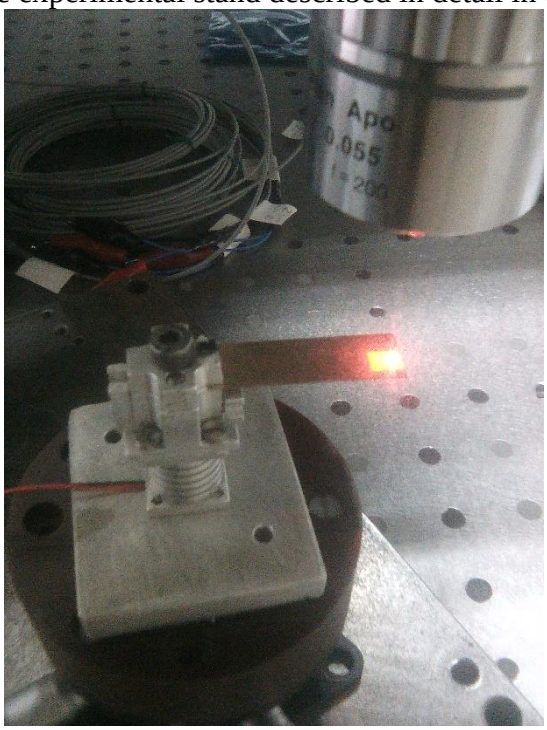

Fig. 4.25. Measuring the speed of the base and the tip of the lamella

Prin raportul celor două mărimi s-a obținut graficul funcției de transfer a sistemului, prezentat în 4.26.

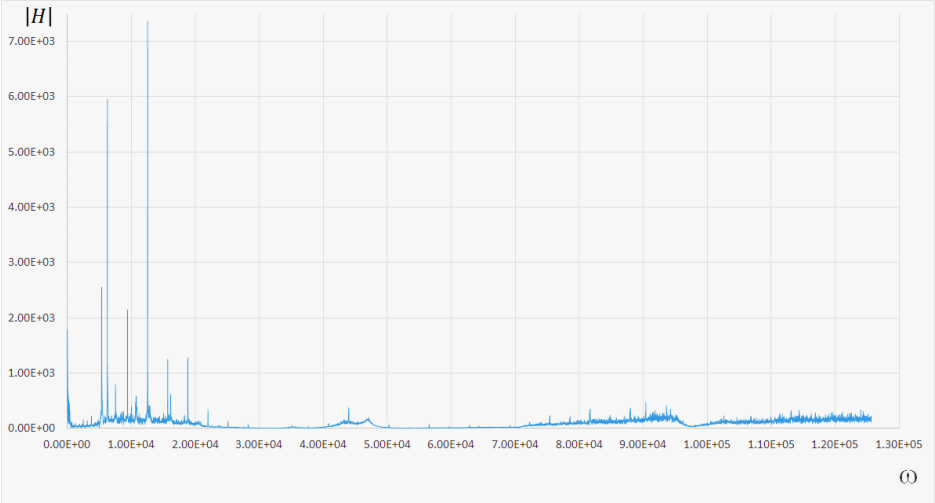

Fig. 4.26. System transfer function

To determine ωmax the relation applies:

$$H'(\omega) = 0 \rightarrow -\frac{m\omega_{max}(c^2 m{\omega_{max}}^4 + 2k^2 m{\omega_{max}}^2 - 2k^3)}{\sqrt{c^2{\omega_{max}}^2 + k^2}((k - m{\omega_{max}}^2)^2 + c^2{\omega_{max}}^2)^{\frac{3}{2}}} = 0 \quad (4.2$$

Results:

$$\omega_{max} = \sqrt{\frac{\sqrt{k^3 m(2c^2 + km)} - k^2 m}{c^2 m}} \quad (4.2$$

The maximum value of the amplitude Rmax, corresponds to the graph in fig. 4.26., The value of ωmax.

Thus:

$$H(\omega_{max}) = R_{max} \quad (4.3$$

Results the value of the maximum amplitude:

$$R_{max} = \sqrt{\frac{c^4\sqrt{k^3 m(2c^2 + km)}}{2m^3 k^4 + (c^4 - 2kc^2 - 2k^2 m)\sqrt{k^3 m(2c^2 + km)}}} \quad (4.3$$

For the calculation of the damping it is necessary to determine the bandwidth corresponding to an attenuation of 3dB below the maximum value of the amplitude. The segment of the graph in fig. 4.26. which corresponds to the maximum amplitude has been increased, in order to be able to observe the required bandwidth.

The determination of the bandwidth is presented in 4.27.

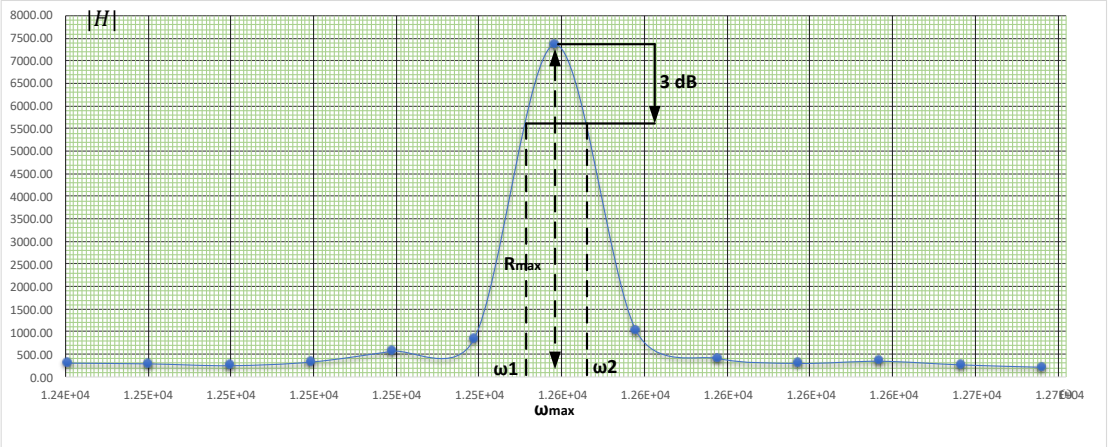

Fig. 4.27. Determining the bandwidth

The 3 dB attenuation is approximately equal to √2 / 2 of the maximum amplitude value. Therefore, the relation that determines the bandwidth abscissas, ω1 and ω2 can be written:

$$\frac{\sqrt{k^2+\omega^2c^2}}{\sqrt{(k-m\omega^2)^2+\omega^2c^2}} = \frac{\sqrt{2}}{2}\sqrt{\frac{c^4\sqrt{k^3m(2c^2+km)}}{2m^3k^4+(c^4-2kc^2-2k^2m)\sqrt{k^3m(2c^2+km)}}} \quad (4.3$$

ω1 and ω2 are the two real and positive solutions of equation 4.32.

4.3. MODELING AND SIMULATION OF STATIC OPERATION

The static operation of the proposed sensor is based on the variation of the inductance of the coil, depending on the change of the magnetic flux in its coils. The calculation relation of the inductance of a spiral plane coil is of the form:

$$L = N\frac{\Phi}{I} \quad (4.3$$

Where:

N = the number of turns of the coil,

Φ = magnetic flux through the coil

I = electric current intensity

The inductance of the sensor coil was first determined using the finite element method and COMSOL Multiphysics software. For this purpose, it was necessary to make a modified sensor model, in which the linear coil supply terminals were extended to the limit of the air body that closes the magnetic field. This modification was necessary in order to be able to use a Terminal type condition at the air-coil boundary (fig. 4.28).

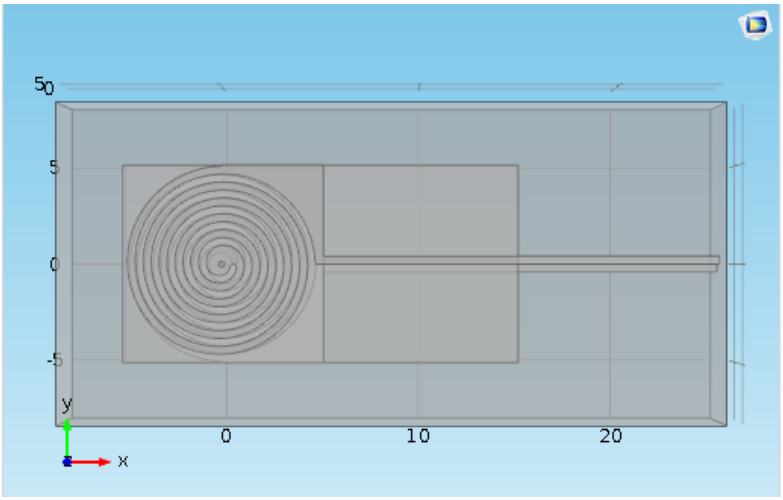

Fig. 4.28. Modified coil model

A voltage V = 0.22 V was applied to the coil terminals, and the working environment used was Magnetic and Electric Fields. The use of another working module was necessary to determine the inductance of the coil, this option not being available in all electromagnetism modules.

Each subdomain of the studied set was discretized separately, using elements of different sizes, depending on the geometry of each subset. This type of discretization ensured the obtaining of precise results, in a relatively short working time.

The distribution of the electromagnetic field of the coil, as well as its inductance are shown in fig. 4.29.

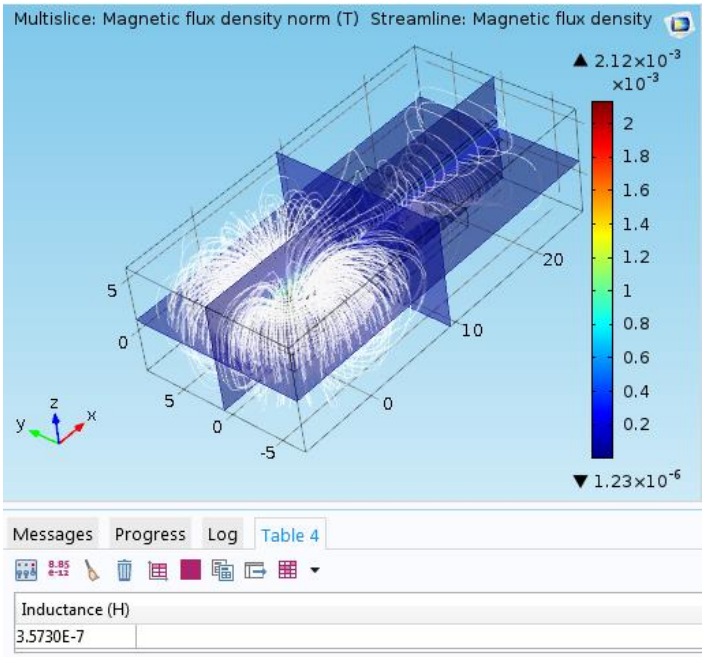

Fig. 4.29. Electromagnetic field distribution and coil inductance

4.4 DETERMINATION OF THE INFLUENCE OF THE POSITION AND THICKNESS OF THE MAGNETIC ELEMENT ON THE COIL INDUCTANCE

4.4.1. The influence of the position of the magnetic element on the inductance of the coil

In order to demonstrate the functionality of the inductive sensor, a numerical calculation model was developed with the help of which the influence of the position of the magnetic plate of the sensor on the inductance of the detection coil is determined. In the same study was determined the influence of the thickness of the magnetic element on the inductance of the coil, as well as the law of variation corresponding to both parameters.

The 3D model of the studied system was made using SolidWorks 2015 software. Initially, the thickness of the magnetic plate was defined with the value of 1 mm, following to vary the distance between the magnetic plate and the detection coil, incrementally, with a step of 0.5 mm

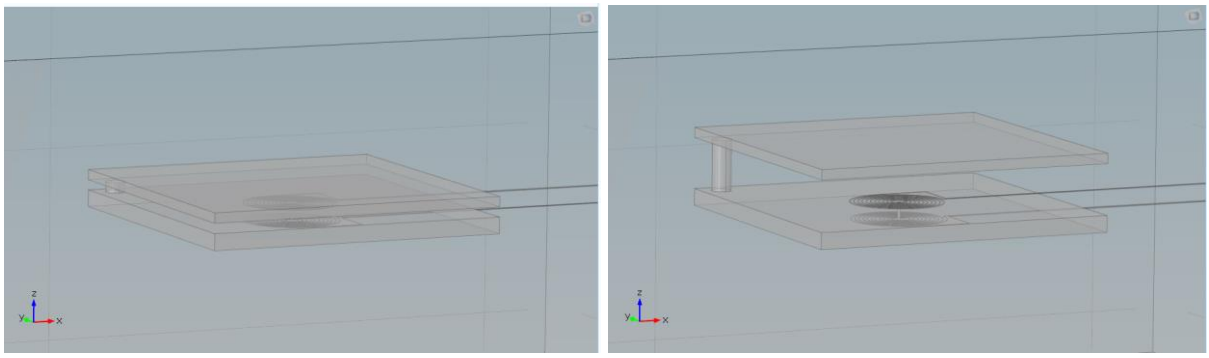

a. b.

Fig. 4.30. Gap of 0.5 mm (a) and 5 mm (b) respectively

In addition to the geometry of the sensor, a circumscribed parallelepiped was added to it, to which air was assigned as material and which is necessary for the delimitation of magnetic field lines.

The variation of the inductance of the coil depending on the distance between it and the magnetic element is shown in the graph in fig. 4.33.

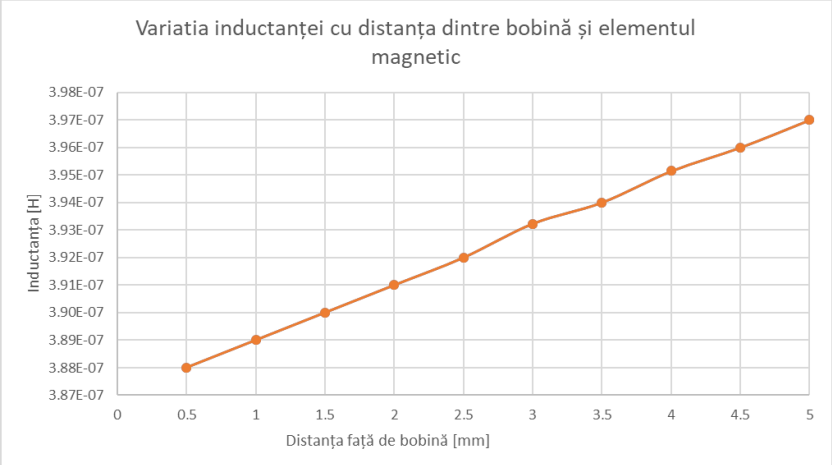

Fig. 4.33. Induction variation

CHAPTER 5: EXPERIMENTAL RESULTS

5.1. THE INFLUENCE OF MANUFACTURING TECHNOLOGIES ON THE MECHANICAL PROPERTIES OF THE NICKEL THAT ENTERS THE STRUCTURE OF THE PROPOSED MICROSENSOR

5.1.1. Introduction

The objective of the study was to determine the dynamic modulus of elasticity of nickel processed by electroplating, in order to obtain a more accurate characterization of the behavior of the moving slide that is part of the MEMS microsensor. In order to achieve the proposed objective, we opted for an analytical determination of the studied parameter, using the equation that describes the resonant frequency of the rectangular shaped beams in the console, existing in the literature. In this sense, the natural frequencies of several microgeams that are part of a plate made by electrodeposition of nickel on a gilded silicon support were determined experimentally. The obtained results were introduced in the analytical model, thus determining the modulus of elasticity of the electrodeposited nickel and highlighting, in parallel, the variation of its value on the x and y axes of the nickel plate, due to the influence of technological parameters.

5.1.2. Description of the experimental stand used

Microscopic visualization and static and dynamic analysis are key aspects of the process of developing and testing MEMS structures. They are indispensable for the validation of finite element calculations and the measurement of surface deformation. The MSA 500 microsystems analyzer (fig. 5.1) was designed to combine several measurement techniques in order to characterize the studied surfaces, as well as to determine the displacements in and out of the studied structure.

Fig. 5.1. Microsystems analyzer MSA 500 (Polytec)[52]

The Polytech MSA 500 uses optical techniques for non-contact measurement of the shapes and displacements of structures on the 3 axes: Laser-Doppler vibrometry for out-of-plane measurements, stroboscopic video microscopy for displacement in the plane, white light interferometry for high-resolution topography. By integrating all these technologies into the same measuring device, the MSA 500 has become the global standard tool for dynamic characterization of MEMS.

In the design and manufacture of microsystems, a precise verification of the topography of functional surfaces is necessary to ensure the achievement of quality and performance standards. Due to its excellent spatial resolution, both in terms of structure and out of plan, the topography measurement unit, part of MSA 500, is ideal for analyzing the three-dimensional profile of structures.

The measurement principle is based on the interference resulting from the overlap of two monochrome light beams. An LED light source emits a beam that is then divided into two distinct rays, using an optical prism. The reference radius is directed towards a reference surface, and the measuring radius is directed towards the studied surface. The light is then reflected from both surfaces and, depending on the differences, interference fringes are obtained, detected by a camera.

By this method the flatness, parallelism, radii of curvature, angles, volumes, height and roughness of the sample can be determined.

The vibrometer itself is a high-precision optical transducer used to determine vibration frequencies and sample movements. Its operation is based on the detection of the variation of the frequency of a light radiation, reflected by the studied surface. During travel, the sample reflects the light beam previously directed at it, and the Doppler variation of the frequency is used to measure the speed of movement along the axis of the measuring radius.

The internal signal generator periodically excites the component with a sinusoidal or pulse signal. A "model generator" uses a green LED to generate ultra-short flashes of light (<80 ns) synchronized with the phase position of the excitation signal. This results in a high degree of phase accuracy, even in the case of high frequency excitations. The diaphragm of the camera is, in turn, synchronized with the excitation.

This procedure guarantees high measurement accuracy and real-time visual analysis. The system is set to operate in the selected frequency bands following out-of-plane vibration measurements.

The diagram of the measurement method is shown in fig. 5.4.

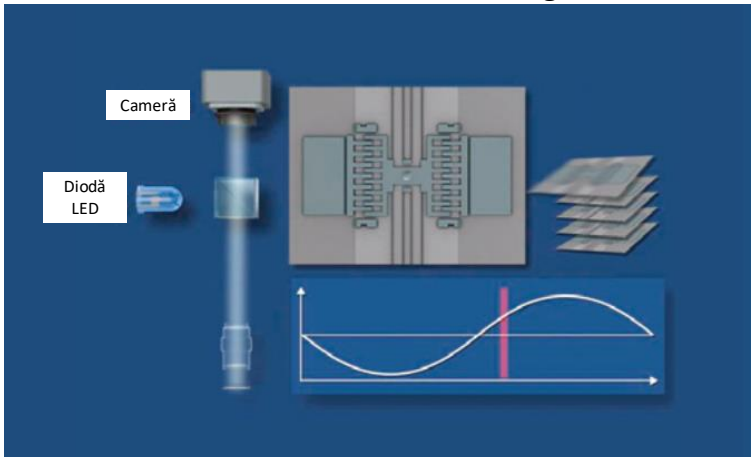

Fig. 5.4. Measurement by stroboscopic video microscopy method [53]

To place the structure in the measuring field, a positioning table with three degrees of freedom is used (fig. 5.5), in order to ensure an appropriate adjustment of the position of the microfeam in which to obtain the best possible reflectivity of the laser beam on the studied area.

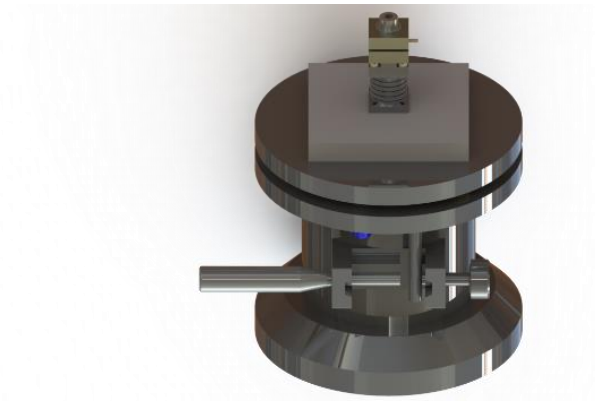

Fig. 5.5. Sample positioning system

During the measurements, it was found that obtaining a good reflectivity on the surface of the structure is relatively difficult to achieve, due to the inaccurate adjustment of the table on the three axes. To eliminate this problem, a new positioning system was designed (fig. 5.6), whose adjustment accuracy will be ensured with the help of micrometric screws.

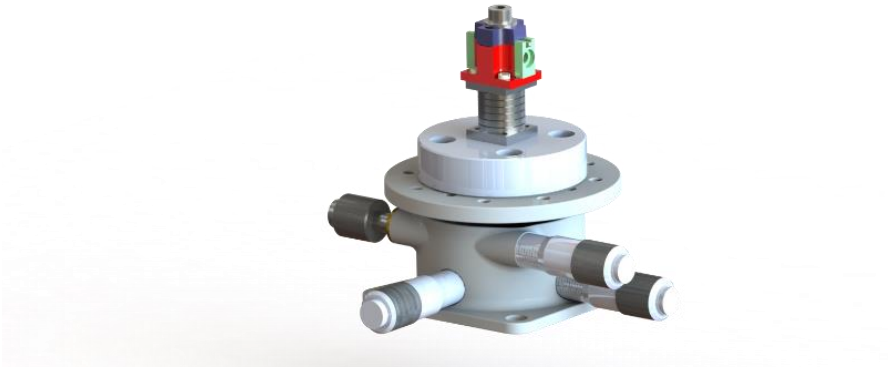

Fig. 5.6. New positioning system used

In order to minimize the effects of a defective grip of the structure on the measurement results, a special construction vise was used to fix the samples on the positioning table (fig. 5.7). The main objectives pursued in the design and realization of the clamping device were to obtain the most efficient grip of the samples and to maintain the parallelism of the vise in order to achieve the highest level of reflectivity of the laser beam on the surface. As such, the vise clamping surfaces were made by high-precision cutting processes, followed by a grinding process and rigorous metrological checks.

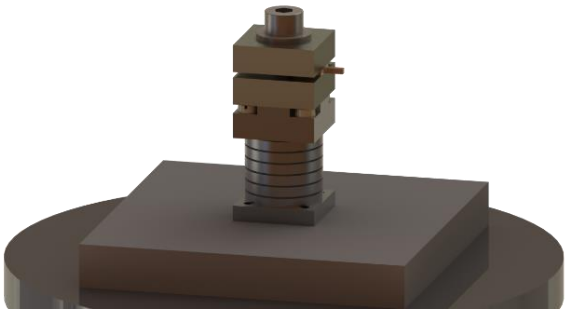

Fig. 5.7. The sampling device and the piezoelectric actuator used

It was found that although the sampling device meets the conditions listed above, the proper fixing of the parts is a relatively difficult and inaccurate procedure, which can introduce possible errors in the measurement results. In order to compensate for this disadvantage, a new clamping device has been designed (fig. 5.8), which ensures, in addition to increased stability and adequate fixation of the samples.

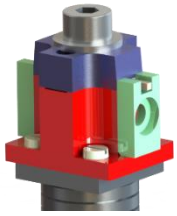

Fig. 5.8. New sample holding system

5.1.3. Description of the tested samples

To obtain the test samples, a Ni plate was made by electroplating the metal on a gilded silicon support. The support was made by LIGA technology with laser beam, which has the same quality results as the process based on UV rays, but with much lower costs.

The studied beams were cut from the Ni plate thus obtained, by a wire EDM process. It was preferred to obtain all the microstructures from the same Ni plate, in order to avoid the possible variations of the mechanical properties of the material induced by the use of individual molds.

To study the variation on the surface of the plate of the dynamic modulus of elasticity of the deposited nickel, one set of samples was oriented along the x-axis of the plate and another along the y-axis. The shape of the base of the microfeamers in the console differs depending on their orientation, to facilitate their identification. To check whether the variation of this parameter occurs even if the x- and y-oriented samples have close positions on the plate, an additional set of samples was created, in which the x and y microgeams alternate within the same row (fig. 5.11).

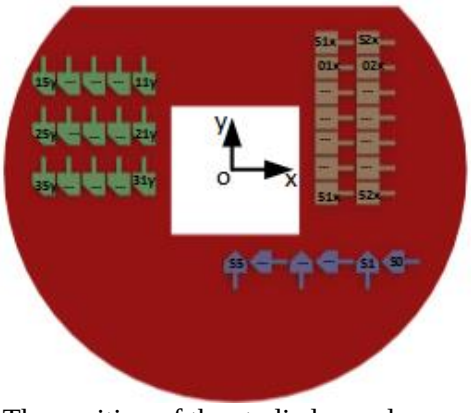

Fig. 5.11. The position of the studied samples, on the Ni plate

5.1.4. Test method

The resonant frequency of the microfeamers in the console was determined using the Polytech MSA 500 microsystems analyzer, by the method of laser - Doppler vibrometry. The interferometer generates two laser beams: a reference one, positioned in the microscope field using the dedicated software and a measuring one, which during the data acquisition process scans a network of points, initially established by the user.

After bringing the vibrometer to the optimal operating parameters by adjusting as precisely as possible the position of the structure relative to the emitted laser beam, with the help of specialized software a network of measuring points is generated. In the case of the studied structures, a network of rectangular points was chosen, corresponding to the geometry of the structure (fig. 5.12). The density of the measuring points is chosen by the user, and it is recommended to have a sufficiently high value to obtain an accurate measurement.

Subsequently, during the measurement process, the laser beam will scan each of these points, in order to obtain the frequency band and the shapes of the vibration modes of the microstructures.

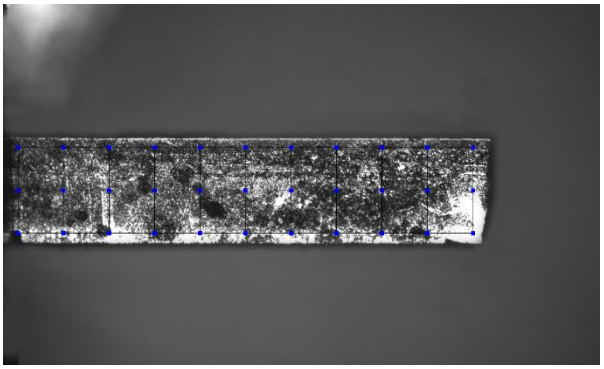

Fig. 5.12. Network of measurement points for one of the studied micro-beams

A piezoelectric actuator shown in fig. 5.6. It was operated using a pseudo-random signal, with an amplitude of 0.5 and a frequency of 50 kHz.

Figure 5.13 shows the shape of the first vibration mode of one of the studied structures, together with the frequency spectrum. The cursor indicates the resonant frequency of the beam, the value of which is shown in the right window.

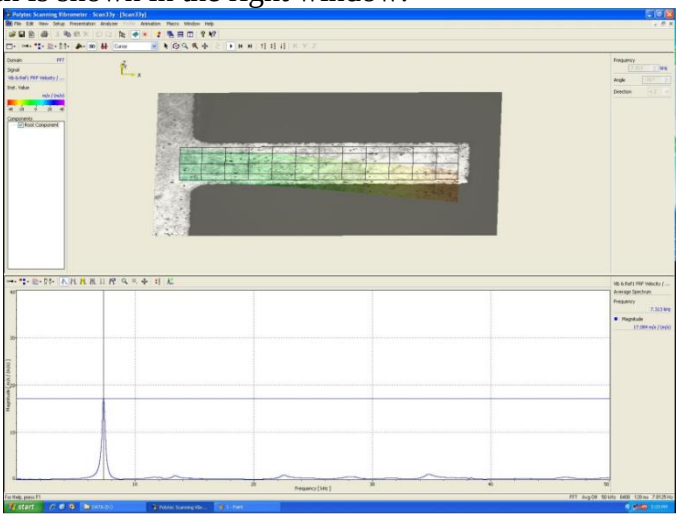

Fig. 5.13. Experimental results

5.1.5. Interpretation of results

The determination of the dynamic modulus of elasticity of deposited Ni was performed by introducing the experimentally determined values in the formula used in the literature to describe the algorithm for calculating the resonant frequencies of rectangular microfeams.

The values of Young's modulus determined according to the described algorithm were divided by an EE constant, representing the value of the dynamic modulus of elasticity of a similar structure of larger dimensions, obtained by the same technological process.

Based on the results obtained, a comparison was made between the E / EE ratio values for the studied beams, in relation to their position on the Ni wafer. The comparison had the role of highlighting the variation on the plate surface of the Young's modulus of the deposited material, and its results are presented in fig. 5.14.

The x-axis of the graphs corresponds to the position of the samples on the plate, where 0 represents the center of the plate, and the dynamic modulus of elasticity is represented on the y-axis.

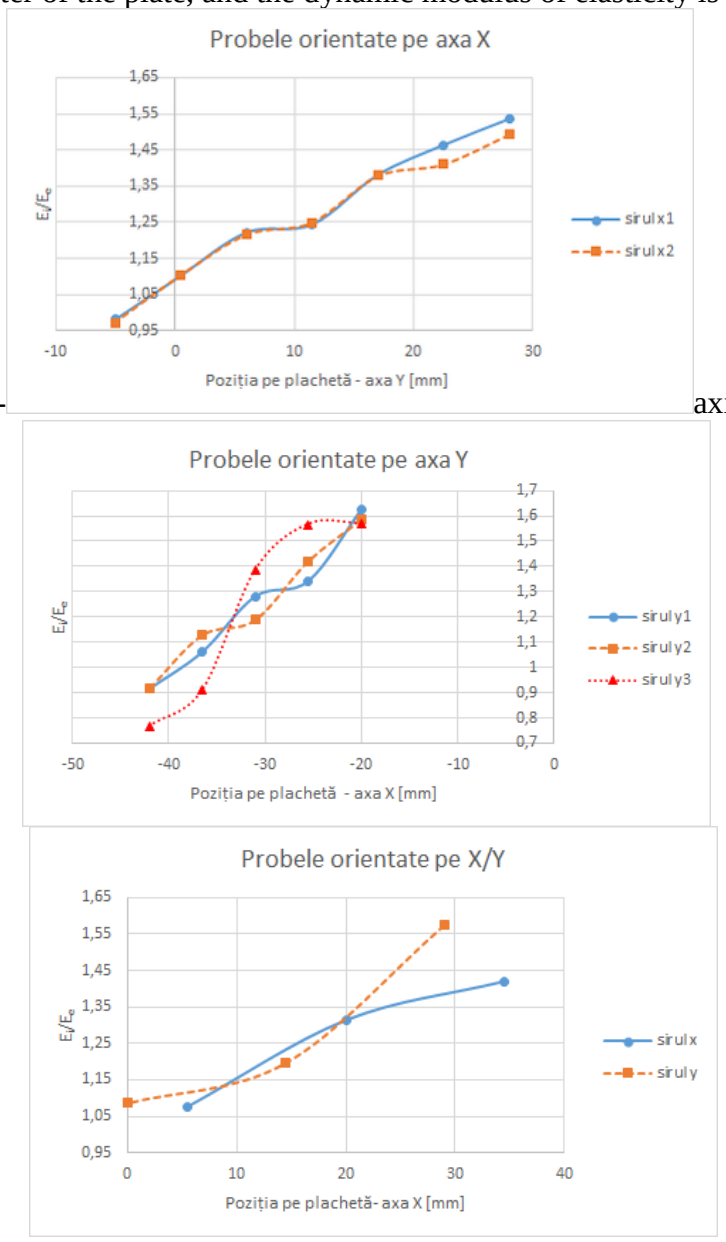

Fig. 5.14. Variation of Young's modulus depending on the position of the micro-beams on the plate

It can be seen that for x-axis oriented micro-beams, no major differences appear between the two rows of samples. The E / EE ratio increases with the distance between the center of the platelet and the sample studied, in the direction of OY.

In the case of samples oriented in the y direction, the E / EE ratio decreases from the center of the plate in the OX direction. The largest variation is recorded for the 11y-15y series of samples. The analysis of the variation of the plate thickness indicated the existence of a relationship between this parameter and the value of the dynamic modulus of elasticity. Thus, Young's modulus has higher values in the case of low thickness samples. This aspect is explained by the fact that the thicker samples resulted from a higher density of the electrolysis current, which led to the obtaining of areas with spongy structure, of low rigidity.

For samples alternately oriented on x and y, it can be seen that the differences between the values of each set of samples are small and the E / EE ratio increases with the distance from the center of the platelet.

5.2. DETERMINATION OF THE FREQUENCY RESPONSE OF MORE MOBILE LAMELLA CONFIGURATIONS

For the subsequent realization of the miniature version of the proposed sensor, several configurations of the flexible lamella were tested, in order to determine its optimal configuration. The test pieces are made of brass, with various sizes.

The first set of parts (1-7) have the inertial mass attached to the fixed edge of the lamella by two fasteners, and the second set (8-14) uses a single fastener. The microscopic image of a section of both types of parts is shown in fig. 5.16.

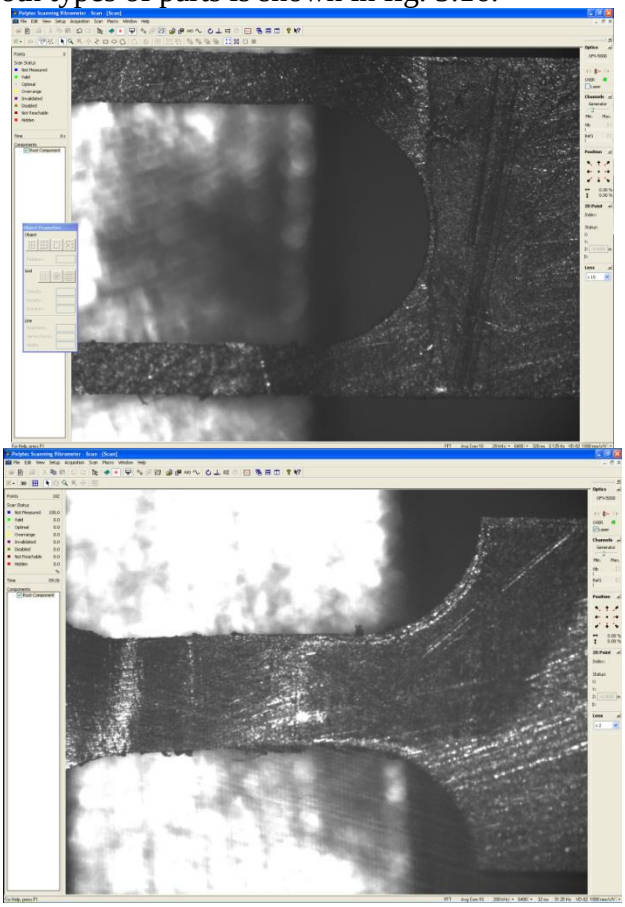

Fig. 5.16. Microscopic image with both types of parts

I determined the resonant frequencies of each piece, using a numerical model made using COMSOL Multiphysics software. The resonant frequencies and vibration modes obtained were then compared with those determined experimentally, using the same stand described in chap. 5.1.

In fig. 5.17 shows an example of validating the numerical model for calculating the resonant frequencies by comparison with the experimental results.

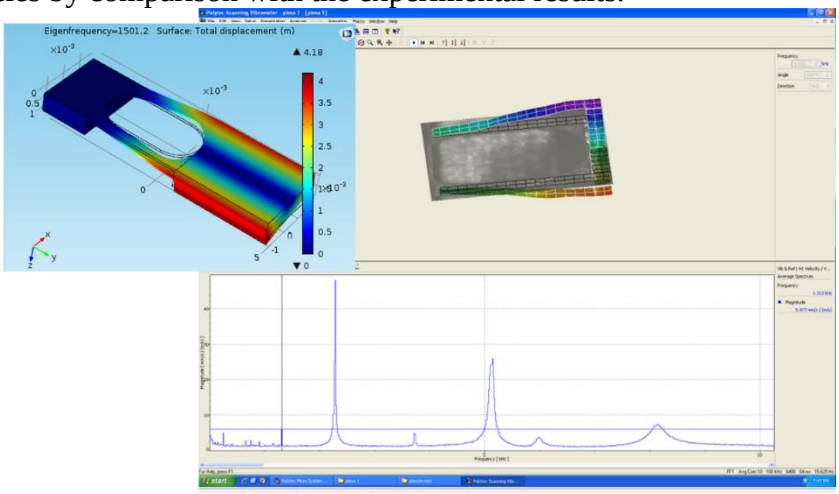

Fig. 5.17. Validation of the model for calculating the resonance frequency through experimental results

5.3. EXPERIMENTAL DETERMINATION OF COIL INDUCTANCE VARIATION DISTANCE BETWEEN COIL AND MAGNET MATRIX LAMELLA

The static operation of the sensor involves the introduction of the coil-movable lamella assembly in a fluid flow, whose impact pressure will cause the deformation of the movable lamella of the sensor. Following the deformation, the distance between the magnets and the coil changes, which causes a variation of the magnetic flux in the coil. Due to the difference in magnetic flux, the inductance of the coil will also register a variation.

The response curve of the coil in relation to the distance between the blades was determined experimentally, in order to validate the numerical model made in the previous chapter.

5.3.1. The experimental stand

An LDC 1614 circuit, produced by Texas Instruments and the dedicated development board, was used to detect the variation of the coil inductance, produced by the proximity and distance of the matrix of permanent magnets.

This circuit is based on the property of some materials to induce a change in the electromagnetic field generated by an inductor. An inductor, together with a capacitor forms an L-C resonant circuit, used to create an electromagnetic field. In the case of an L-C resonator, a disturbance of the electromagnetic field will cause a change in the inductance of the coil leading to a change in the resonant frequency. LDC 1614 integrated circuit, which is a digital signal inductance converter that measures the frequency oscillation of an L-C resonator. The electronic device will generate a digital value proportional to the resonator frequency, and the measured frequency can be converted into an equivalent inductance.

The measuring stand used is shown in fig. 5.20.

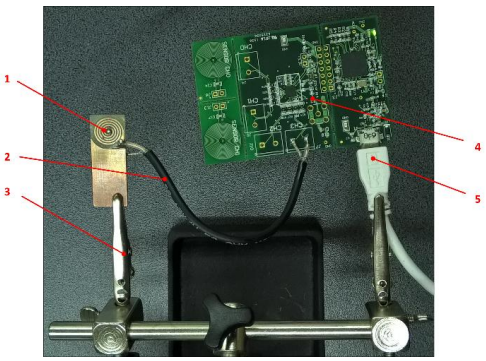

Fig. 5.20. The experimental stand

The sensitive element (coil) (1) is electrically connected to the LDC 1614 EVM board (4) via the shielded cable (2). Data is collected by a PC via the connection (5). The whole electronic assembly is supported by the support (3).

The coil is made on a double layer printed circuit board, the distance between the layers being 1,524mm.

The signal is taken from the coil to minimize interference by a shielded cable that is attached to one of the input channels of the integrated integrated circuit LDC1614 for converting the inductance into a digital signal that has a resolution of 28 bits.

5.3.2. The results obtained

The first stage of the tests consisted in determining the inductance of the coil in the absence of the permanent magnet matrix and comparing the value obtained with the numerical calculation model.

The coil inductance value is 0.385 μH, which thus validates the numerical calculation model in fig. 4.29, in which an inductance value of 0.387 μH was obtained.

The next step of the test was to insert the permanent magnet lamella, which was positioned in turn at distances between 1.4 and 3 mm of the coil, with a pitch of 0.1 mm, and the inductance of the coil was measured in each case. For the precise adjustment of the positioning of the movable blade in relation to the coil, a positioning system with micrometric screw was used. The experimental stand used is shown in fig. 5.22.

Fig. 5.22. Magnet lamella positioning system

5.3.3. Interpretation of experimental results

After measuring the inductance in each position, the response curve of the coil was determined according to the distance between it and the moving element. The variation of the inductance with the interstice between the elements is presented in fig. 5.23.

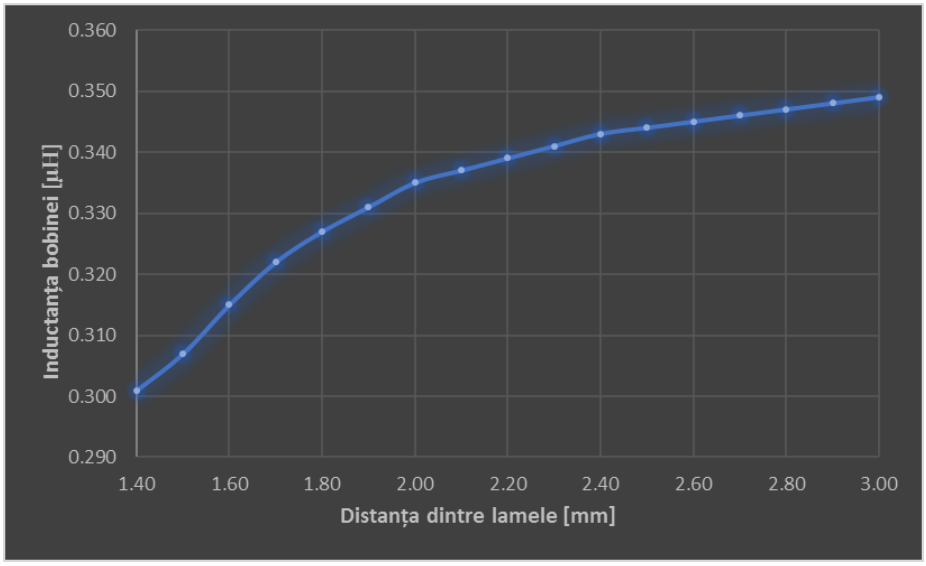

Fig. 5.23. Sensor response curve

From fig. 5.22 a decrease in the inductance of the coil can be observed with the proximity of the magnetic element to it, which demonstrates the principle of operation of the proposed sensor

CHAPTER 6: CONCLUSIONS, PERSONAL CONTRIBUTIONS, AND FUTURE RESEARCH POSSIBILITIES

6.1. RESEARCH ACTIVITY CONCLUSIONS

The field of interest of this doctorate thiesis consists of studying, optymizing, development and testing of sensory elements of presurre measuring for pneutronic systems of reduced size. The thesis was chosen based of studying from the latest documentation and research paths in the field of smart pneutronic systems, from which I concluded that the main development tendency of pneutronic systems is based on miniaturizing of these systems for incorporating them in the most number of applications.

To complete the first objective of this thesis which would be the modeling and simulation of constructing MEMS type pressure transducers with a classic configuration, I have determined the influence of the geometry of the membrane of these sensors upon their sensibility. With the goal of optimizing the response of piezoresistive transducers, I have developed several calculation models that allow determining the optimal constructive parameters of these sensors. Also, I have developed a new constructive model of the MEMS piezoresistive pressure sensors which allows the increase in sensitivity for the circular membrane transducers.

Another objective of this thesis was the modeling simulation and testing of a new constructive solution for the electromagnetic pressure sensor, with static or dynamic state functioning. The proposed sensor is designed for measuring the dynamic pressure of compressed air, and the functioning of this sensor was designed both analytic and numerical using the finite element method and the COMSOL Multiphysics software. Based on the simulations carried out

it was concluded that optimal functioning of the sensor was in dynamic state, especially when it is used at its first resonant frequency because in the first vibration pattern, the variation of it's own frequency with the pressure of the fluid has a linear characteristic.

The static functioning state of the sensor was tested including experimental measurements of the variation of the coil inductance with the distance between the slides of the sensor. After comparing the results gathered from testing the principle and from those determined through the finite element method, the correctness of the models designed was validated and also the functionality of the constructive solution was validated.

Taking into account that the purpose of this thesis consists mostly of miniature sensors, in chapter no.5 it was determined experimentally the influence of microfabrication technologies on the mechanical properties of materials specific to MEMS transducers. The technology studied was electroplating and it was concluded that the evenness of the material properties on the directions of the plane of the plaque consists in the close connection with the current density used in the electroplating process.

6.2. FUTURE RESEARCH

Within the furture research options stands the testing of the proposed sensor in a simple pneutronic system and the validation of the results gathered with the help of an additional ansamble of transducers.

Also future research will be focused on the development of a MEMS model for the proposed electromagnetic sensor, the first steps of the miniaturing process being already followed through from the experimental deduction of the resonant frequencies of certain contrucive solutions for the mobile slide of the sensor.

6.3. PERSONAL CONTRIBUTIONS

Among the personal contributions of the author of this thesis stand the following :

The development of a numerical calculation model for determening the influence of the geometry of piezoresistive pressure transducers on their sensitivity,

The development of a numerical calculation models destined for constructive optimization of piezoresistive pressure transducers, from a stand-point of the thickness of the elastic membrane and the positioning of the sensitive elements,

The design and simulation of a constructive solution for the piezoresistive pressure transducers, MEMS type, with superior perfomance above the clasicall model,

The proposal of a new type of electromagnetic transducer designed for measuring dynamic pressure in a pneutronic system,

The design of the mathematical model for the proposed sensor, in the case of dynamic state functioning, with determening the modal parameters (m,c,k,),

Establashing through finite element analysis the resonant frequency of the proposed sensor and the variation of this under the influence of a fluid,

The making of a numarical calculation model for determening the coil inductance of the proposed sensor,

The 3D design of new positioning and securing systems for elements tested through the vibrometric laser method,

Establishing experimentaly the influence of curent density utilized in the electroplating processs on the mechanical properties of materials,

Determining experimentaly and numericaly the resonant frequency of brass slides destined for making the miniature model of the proposed sensor,

The experimental testing of the functionality of the proposed and studied electromagnetic transducer within this doctoral thesis.

6.4. PUBLICATIONS

1. Popescu-Cuță, A., Gheorghe V., Comeagă C.D., (2019) Dispozitiv de fixare a structurilor mecanice de mici dimensiuni pentru măsurarea modului de elasticitate prin vibrometrie laser**,** *nr. A/00761/2019* (Cerere de brevet**)**
2. Udrea, I., Kraus, V.F., Popescu-Cuță, A. (2020) Facility Management Platform Sensors Monitoring for Improving Workplace Services, 36th IBIMA International Conference, Granada, Spain (ISBN: 978-0-9998551-5-7) (ISI**)**
3. Udrea, I., Gheorghe, V.I., Avram, M., Petrache, S., Popescu-Cuță, A., Popa, R.T. (2020) Solution for controlling a hydraulic motor using cloud data, E3S Web of Conferences 180, 02013 – 2020 (ISI)
4. Popescu-Cuță A., Comeagă C.D., Donțu O. (2020), Structural optimization of a MEMS piezoresistive pressure sensor with circular membrane, UPB Scientific Bulletin, Mechanical Engineering Section – in curs de publicare
5. Moraru, E., Donțu O., Besnea, D., Rizescu, C., Rizescu, D., Popescu-Cuță, A. (2019) Experimental Researches Regarding Mechanical Behaviour of Dental Prototypes realized by Additive Technologies, MATEC Web of Conferences. 290. 03011. (ISI)
6. Popescu-Cuță, A., Gheorghe, G., Gheorghe, V., Comeagă, C. D., & Donțu, O. (2016). Optimization Of Pressure Transducers With Silicon Membrane, Regarding Piezoresistors Position. Mecahitech
7. Popescu-Cuță, A., Donțu O., Comeagă C.D., Gheorghe V. (2016) Design and optimization of a low cost MEMS piezorezistive pressure transducer for pneumatic systems, International Conference on Intelligent Computing, Mechanical and Production Processes, Pattaya (Thailand)
8. Gheorghe V., Popescu-Cuță, A., Comeagă C.D., Ilie C. (2015) Determining The Young Modulus Of Electroplated Ni Using Modal Analysis, 7th International Conference on Innovations, Recent Trends and Challenges in Mechatronics, Mechanical Engineering and New High-Tech Products Development MECAHITECH 2015
9. Avram, M., Donțu O., Bucșan, C., Popescu-Cuță, A. (2014) Multi-sensorial Module for Pneumatic and Hydraulic Systems – Concept and Functioning, 6th International Conference on Innovations, Recent Trends and Challenges in Mechatronics, Mechanical Engineering and New High-Tech Products Development MECAHITECH 2014.
10. Avram, M., Popescu-Cuță, A., Bucșan, C., Apostolescu, T.C. (2014) Aspects Regarding The Integration Of Sensors And Transducers In The Construction Of The Hydraulic And Pneumatic Equipment For Automation, 6th International Conference on Innovations, Recent Trends and Challenges in Mechatronics, Mechanical Engineering and New High-Tech Products Development MECAHITECH 2014.
11. Popescu-Cuță, A., Donțu O., Ionașcu G., Avram, M., Comeagă C.D., Manea, E. (2014) Modal analysis of a MEMS cantilever, Advanced Concepts in Mechanical Engineering I, Vol. 658, ISBN-13: 978-3-03835-271-6
12. Avram, M., Bucșan, C., Duminică, D., Popescu-Cuță, A. (2014) Advanced Concepts in Mechanical Engineering I, Vol. 658, ISBN-13: 978-3-03835-271-6

References

1. Krivts, I. L., & Krejnin, G. V. (2016). Pneumatic actuating systems for automatic equipment: structure and design. Crc Press.
2. Avram, M., Banu, V., Bucşan, C., Duminică, D., Gheorghe, V., & Bogatu, L. (2009). Original Solutions of Linear and Rotary Pneutronic Units, 1ST International Conference on Innovations, Recent Trends and Challenges in Mechatronics, Mechanical Engineering and New High Tech Products Development.
3. Avram, M. (2014). Hidronica și pneutronica. UPB DMMP.
4. Smaoui, M., Brun, X., & Thomasset, D. (2006). A study on tracking position control of an electropneumatic system using backstepping design. Control Engineering Practice, 923–933.
5. Thomas, B., Maul, G., & Jayawiyanto, E. (2005). A novel, low-cost pneumatic positioning system. Journal of manufacturing systems, 24(4), 377–387.
6. Avram, M., & Bucşan, C. (2009). Pneutronic Positioning Unit Part 1: Design And Working Principle. Romanian Review of Precision Mechanics, Optics and Mecatronics, 36(19).
7. Avram M., Dumincă D., Udrea C., Gheorghe V., (2008). Hidronica si pneutronica - Aplicații, Editura Universitară, București
8. Zeljko, S., Zilie, T., & Essert, M. (2007). High speed solenoid valves in pneumatic servo applications. Control & Automation, MED'07.
9. Avram, M., Bucşan, C., Duminică, D., & Spânu, A. (2013). On Integrating Sensors Within Pneumatic Equipment. Romanian Review Precision Mechanics, Optics & Mecatronics, (44).
10. Kato, T., Kawashima, K., Funaki, T., Tadano, K., & Kagawa, T. (2010). A new, high precision, quick response pressure regulator for active control of pneumatic vibration isolation tables. Precision Engineering, 34(1), 43-48.
11. Lineaire aandrijving met wegmeetsysteem. (n.d.). din https://www.festo.com/cat/nl-be_be/products__82552.
12. Dolga, V. (2015). Senzori și sisteme senzoriale. Universitatea Politehnica Timișoara.
13. Zet, C. (n.d.). Senzori și traductoare - Lucrare de laborator. Din http://iota.ee.tuiasi.ro/~czet/Lucrari%20de%20laborator/SenzTrad/L6%20TRADDEPLREZ.pdf.
14. Cenuse, L. (n.d.). Suport de curs: Tipuri de traductoare. Din https://portal.ctcnvk.ro/suporturi-de-curs/Arhiva/cenuse-lavineta-suporturi-de-curs Colegiul tehnic de comunicații Nicolae Vasilescu Karpen
15. Tan, K. K., & Putra, A. S. (2010). Drives and control for industrial automation. Springer Science & Business Media.
16. AzoSensors. (2012, May 5). An Introduction to Hall Effect Sensors. Din https://www.azosensors.com/article.aspx?ArticleID=16.
17. Traductoare Hall si utilizarea lor la autoturisme. (n.d.). Din http://www.creeaza.com/tehnologie/electronica-electricitate/Traductoare-Hall-si-utilizarea138.php.
18. Lion Precision. (n.d.). Eddy Current Sensors. Din http://www.lionprecision.com/eddy-current-sensors/.
19. Vornicu, L. (n.d.). Curs senzori și traductoare. Din http://ep.etc.tuiasi.ro/site/Senzori_si_Traductoare/Cursuri/senzori_4.pdf. Universitatea Tehnica Gheorghe Asachi din Iasi.
20. Thermocouples-What is a thermocouple-Types of thermocouples. (n.d.). Din http://www.thermocoupleinfo.com/.

21. NTC thermistor | Resistor types | Resistor Guide. (n.d.). Din https://eepower.com/resistor-guide/resistor-types/ntc-thermistor/.
22. Fraden, J. (2004). Handbook of modern sensors: physics, designs, and applications. Springer Science & Business Media
23. http://ime.upg-ploiesti.ro/attachments/article/102/EA%20cap3.pdf.
24. Haron, S., Sulaiman, H. (2014). Process instrumentation, University of technology Malaysia
25. http://www.workaci.com/pdf/technotes/pressure_technical_notes.pdf
26. Yu, L., Kim, B. J., & Meng, E. (2014). Chronically implanted pressure sensors: challenges and state of the field. Sensors, 14(11), 20620-20644.
27. http://electronicdesign.com/
28. http://www.kulite.com/
29. http://www.sensorsmag.com/
30. http://www.columbia.edu/cu/fowlerlab/fops.html
31. Luque, A., & Quero, J. M. (2005). Modeling and numerical simulation of a MEMS pneumatic valve. In Conference on Electron Devices, 2005 Spanish (pp. 489-493). IEEE.
32. http://nfpahub.com/events/wp-content/uploads/sites/2/2015/10/7-1-Hargus-UMN-MEMS-Pneumatic-Valve.pdf
33. Gorissen, B., Donose, R., Reynaerts, D., & De Volder, M. (2011). Flexible pneumatic micro-actuators: analysis and production. Procedia Engineering, 25, 681-684.
34. Anderas, E. (2012). Advanced MEMS pressure sensors operating in fluids. Acta Universitatis Upsaliensis Uppsala.
35. https://en.wikipedia.org/wiki/Piezoresistive_effect
36. https://en.wikipedia.org/wiki/Hooke%27s_law
37. Lin, L., & Yun, W. (1998). Design, optimization and fabrication of surface micromachined pressure sensors. Mechatronics, 8.5, 505–519.
38. Popescu-Cuță, A., Gheorghe, G., Gheorghe, V., Comeagă, C. D., & Donțu, O. (2016). Optimization Of Pressure Transducers With Silicon Membrane, Regarding Piezoresistors Position. Mecahitech.
39. http://www.efunda.com/formulae/solid_mechanics/mat_mechanics/hooke_plane_stress.cfm
40. Johns, G. K. (2006). Modeling piezoresistivity in silicon and polysilicon. Journal of Applied Engineering Mathematics.
41. https://studylib.net/doc/18349828/piezoresistive-pressure-sensors
42. http://www.learnengineering.org/2012/12/what-is-von-mises-stress.html
43. Popescu-Cuță A., Gheorghe Gh., Gheorghe V., Comeagă C.D., Donțu O. (2020), Structural optimization of a mems piezoresistive pressure sensor with circular membrane, Buletinul științific UPB (în review)
44. Necula, C., Gheorghe, G., Gheorghe, V., Comeaga, D. C., & Dontu, O. (2016). Electromagnetic Multifunctional Stand For Mems Applications. Mecahitech.
45. J.K. Luo, A.J. Flewitt, S.M. Spearing, N.A. Fleck, Milne, W.I., Young's modulus of electroplated Ni thin film for MEMS applications.
46. Spearing, S. M. (2000). Materials issues in microelectromechanical systems (MEMS). Acta Materialia, 48.1, 179–196.
47. http://www.hysen.com/
48. Polytech MSA 500 User Manual
49. Reitz, J., Milford, F., & Christy, R. (2008). Foundations of electromagnetic theory. Addison-Wesley Publishing Company.
50. COMSOL AC/DC Module User Guide
51. Ivas, S. (2003). Teoria macroscopică a câmpului electromagnetic. Editura Fundației Universitare "Dunărea de Jos.".

52. http://www.matweb.com/search/AdvancedSearch.aspx
53. Greenwood, J. C. (1984). Etched Silicon Vibrating Sensor. J. Phy. E. Sci. Instrum., 17, 650–652.
54. Kinnell, P. K., Ward, M. C. L. , Craddock, R. (2004) Physical characterisation of selective stress coupling for resonant pressure sensors Sensors and Actuators A: Physical 115.2: 230-234.
55. Greenwood, J. C. (1988). Miniature silicon resonant pressure sensor. IEE Proceedings D-Control Theory and Applications, 135(5).
56. http://www.sensorland.com/HowPage007.html
57. Luo, Z. et al. (2014) A High-Q Resonant Pressure Microsensor with Through-Glass Electrical Interconnections Based on Wafer-Level MEMS Vacuum Packaging, Sensors 14.12: 24244-24257.
58. http://mech.vub.ac.be/avrg/publications/ModalAnalysis.pdf